e-vectoorc
Electric-Vehicle Control of Individual Wheel Torque for On- and Off-Road Conditions
01 September 2011 - 31 August 2014

The research receives funding from the European Community Seventh Framework Programme (FP7/2007-2013) under grant agreement No 284078

E-VECTOORC

Electric Vehicle Control of Individual Wheel Torque for On- and Off-Road Conditions

FP7-INFSO-284078

Deliverable D7.2
Test Vehicle

Authors / Contacts	Editor: Phil Barber (JLR) Kevin Verhaege (Inverto) Aldo Sorniotti, Leonardo de Novellis (Surrey) Thomas Putz (TRW) Javier Orus(ITA)
Responsible of the deliverable	Phil Barber (JLR) Phone: +44 7787 285137 Email: pbarber2@jaguarlandrover.com
Target Dissemination Level	**CO** (Confidential, only for members of the consortium (including the Commission Services))
Status of the Document	Final Version

The research receives funding from the European Community Seventh Framework Programme (FP7/2007-2013) under grant agreement No 284078

Revision History

Revision	Date	Description	Issued by
0.5	30th April	Intermediate draft for comment	Phil Barber
0.6	7th May	Final draft for comment	Phil Barber
0.8	30th May	Update	Phil Barber
1.0	12th June	Update	Phil Barber

Abstract

This document summarises the main activities and results related to Task 7.2 of the E-VECTOORC project. This is the build of the demonstrator vehicle. The report presents the activities related to the vehicle modifications, the traction and brake system. The cooling system and the range extender trailer are also described. The report contains the results of experiments to validate the requirements of the traction system and of the dynamic response of the brake and motor systems.

The research receives funding from the European Community Seventh Framework Programme (FP7/2007-2013) under grant agreement No 284078

Table of Contents

The research receives funding from the European Community Seventh Framework Programme (FP7/2007-2013) under grant agreement No 284078

The research receives funding from the European Community Seventh Framework Programme (FP7/2007-2013) under grant agreement No 284078

1 Introduction

The E-VECTOORC vehicle demonstrator has been produced by Flander's Drive and delivered to the consortium. This report describes the details of the vehicle. It also includes some additional information relating to the delivery of the vehicle, in particular:

Section 2: Vehicle specifications

Section 3: Performance of the electric motors

Section 4: The range extender trailer

Section 5: Experimental analysis of the actuator dynamics

Concluding remarks presented in section 6 highlight that the vehicle has been delivered and is suitable for control studies in the rest of the project.

2 Vehicle Specification

This section describes the E-VECTOORC vehicle demonstrator (Figure 2.1).

Figure 2.1 - E-VECTOORC test vehicle during limit handling tests with two wheel drive in project year 2

The vehicle powertrain consists of 4 switched reluctance motors each with a specific switched reluctance inverter unit. The drivetrain is connected to a 600 Volt battery pack. The main motor generator unit is controlled by a dSPACE MicroAutoBox.

The vehicle is intended for vehicle dynamics and capability research. It is not intended to demonstrate all weather, wading or off-road (tyre) traction studies. The vehicle will only be operated in 'clean' environments such as test tracks and technical test areas.

The research receives funding from the European Community Seventh Framework Programme (FP7/2007-2013) under grant agreement No 284078

2.1 Vehicle Dimensions

An overview of the vehicle dimensions is given in Table 2.1.1.

Table 2.1.1 - Vehicle dimensions

Type	Land Rover Range Rover Evoque 5-doors
Mass	2105 kg (empty mass)
Driveline	Individual 4 wheel drive
Max speed	~190 km/h
Tire size	235/55 R19
Wheelbase	2665 mm
Track width	1625 mm
Drag coefficient	0.35
Frontal surface	2.323 m²
Gear ratio	10.56
Nominal power	121 kW
Peak power	300 kW
Motor type	4 x Switched Reluctance (SR) motors
Battery cell type	Lithium Titanate Oxide
Brakes	Slip Control Boost (brake by wire)
Ambient temp	0 to 40°C
Ambient humidity	45 to 85%, non-condensing

2.2 System High Voltage (traction) Architecture

An overview of the high voltage scheme used on the E-VECTOORC vehicle is given in Figure 2.2.1.

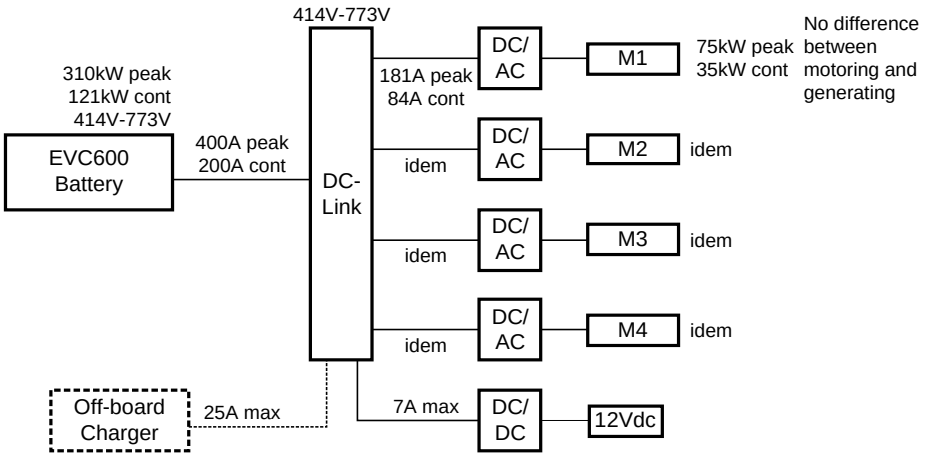

Figure 2.2.1- Block diagram of the E-VECTOORC high voltage architecture

The research receives funding from the European Community Seventh Framework Programme (FP7/2007-2013) under grant agreement No 284078

2.3 Vehicle packaging

Figure 2.3.1 shows the packaging of the motors on the front axle and Figure 2.3.2 shows the setup at the rear. The battery pack is installed in the middle of the vehicle and the control units are installed in the rear of the vehicle (see Figure 2.3.3 and Figure 2.3.4).

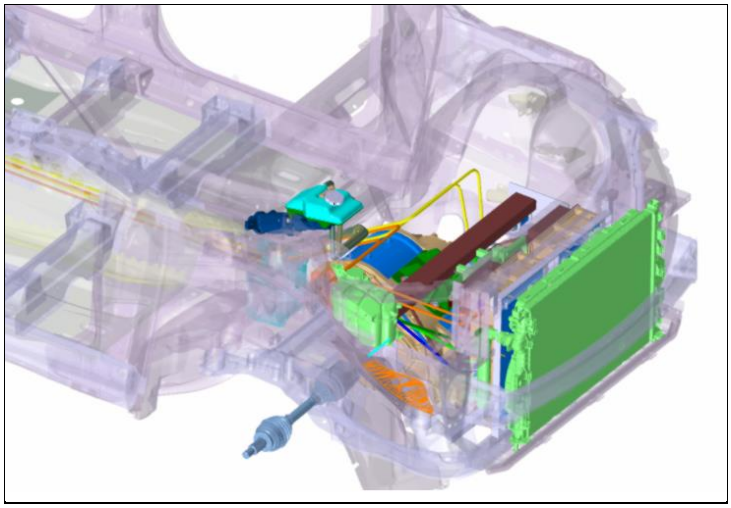

Figure 2.3.1 – Isometric view of front vehicle assembly

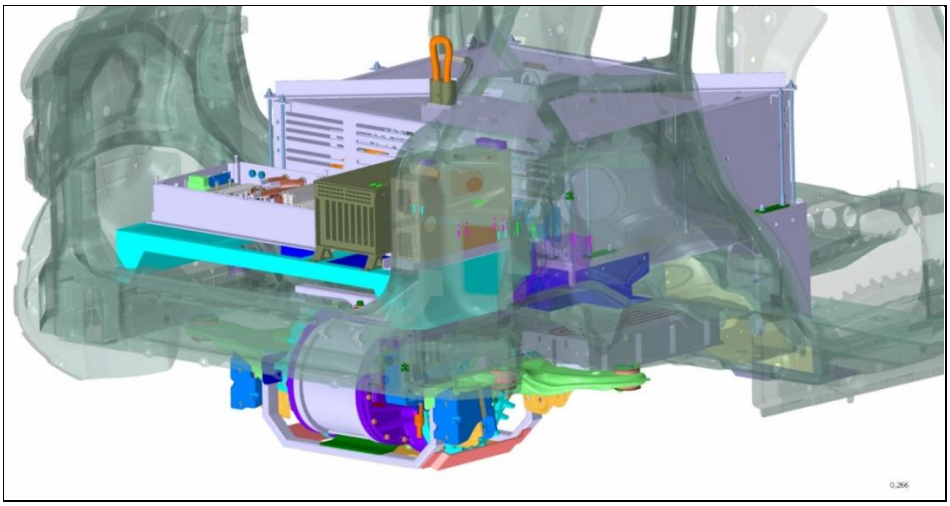

Figure 2.3.2 - Isometric view of rear vehicle assembly

The research receives funding from the European Community Seventh Framework Programme (FP7/2007-2013) under grant agreement No 284078

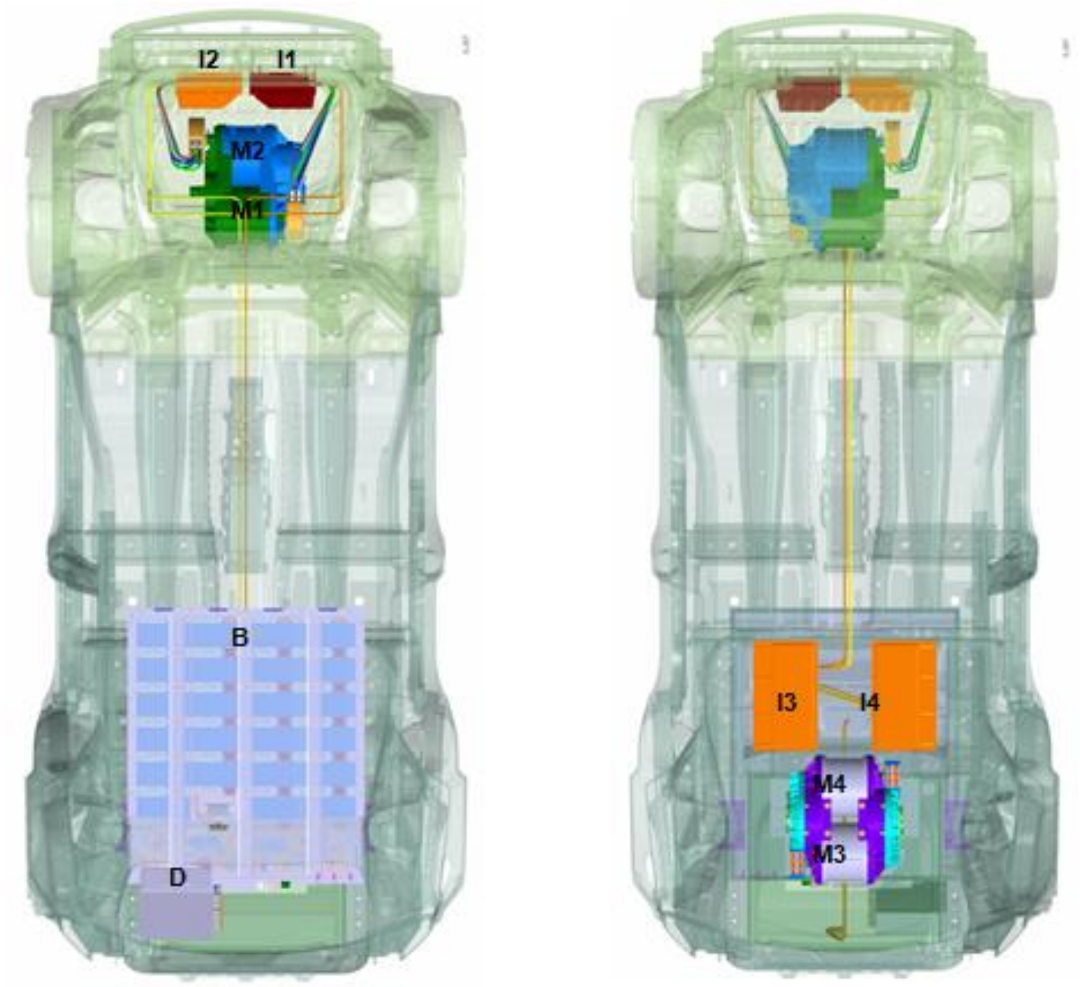

Figure 2.3.3 - Vehicle high voltage top and below views

Legend:

- I1 = SR-Inverter 1
- I2 = SR-Inverter 2
- I3 = SR-Inverter 3
- I4 = SR-Inverter 4
- M1 = SR-Motor 1
- M2 = SR-Motor 2
- M3 = SR-Motor 3
- M4 = SR-Motor 4
- B = Battery pack
- D = Distribution box

Comment: DC/DC to 12V DC is not included in these drawings

The research receives funding from the European Community Seventh Framework Programme (FP7/2007-2013) under grant agreement No 284078

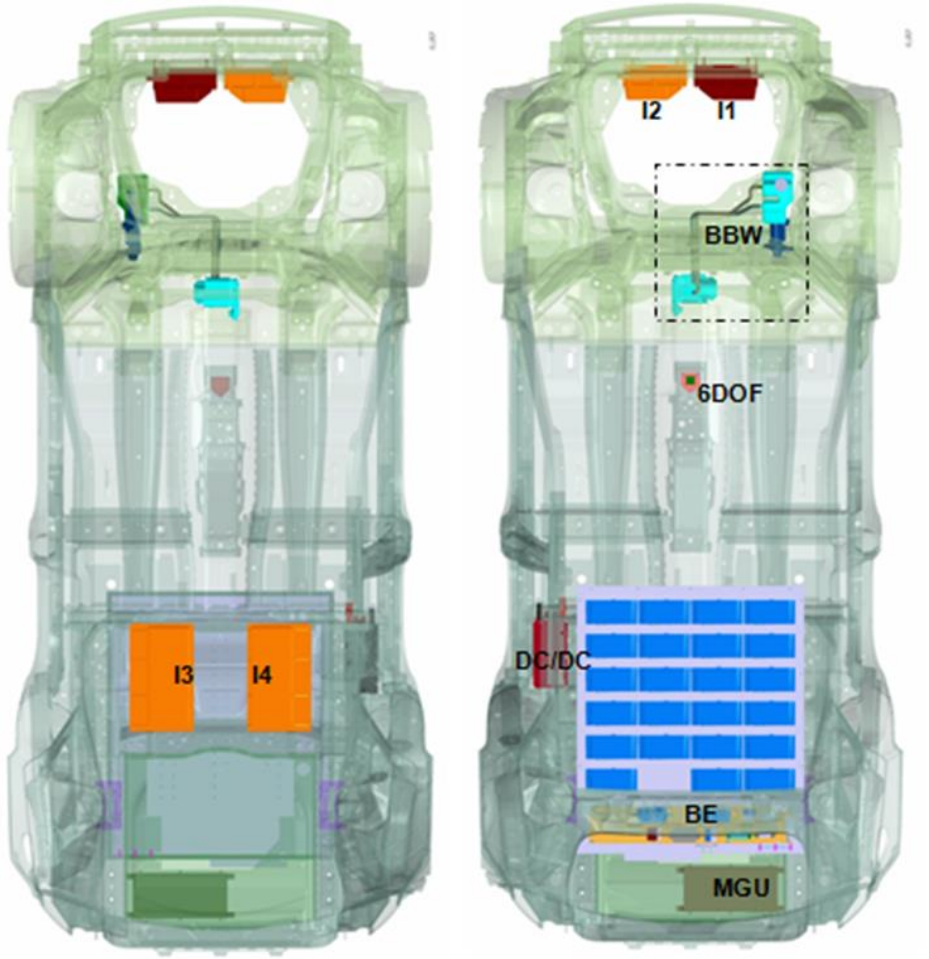

Figure 2.3.4 - Other electric/electronic components, top and below views

Legend:

I1 = SR-Inverter 1
I2 = SR-Inverter 2
I3 = SR-Inverter 3
I4 = SR-Inverter 4
BBW = Brake by wire sysytem
6DOF = Six degree of freedom sensor
BE = Battery electronics
MGU = Motor generator control unit, dSPACE autobox
DC/DC = DC converter to 12VDC

The research receives funding from the European Community Seventh Framework Programme (FP7/2007-2013) under grant agreement No 284078

2.4 Vehicle Components

2.4.1 High voltage system

All high voltage components are linked via the high voltage distribution box. The layout is given in Figure 2.4.1.1.

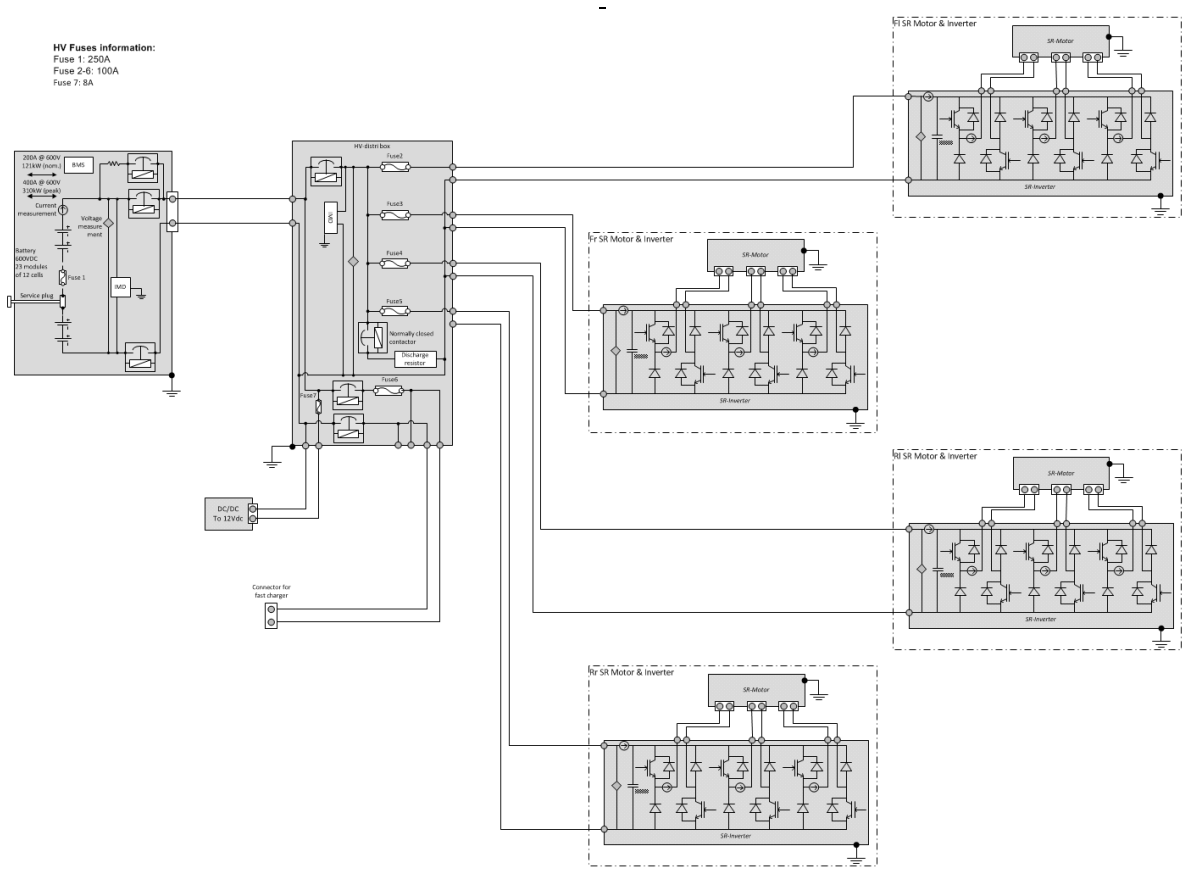

Figure 2.4.1.1 - Vehicle High Voltage Components

2.4.2 In-Vehicle Communication System

The communication busses are shown in Figure 2.4.2.1. The original high speed vehicle CAN-bus is connected to the dSPACE MicroAutoBox (MGU) and an electric speed controllable water pump for the cooling management (CAN-bus 3). The battery management system of the 600 V battery pack, the 2 kW converter from 600 Vdc to 12 Vdc and the 20 kW fast off-board charger are connected with the six degree of freedom sensor (CAN-bus 4). A separate CAN-bus for the four inverters and the MGU allows a maximum communication speed of 2ms time base (CAN-bus 1). There is a private CAN between the MGU and Slip Control Boost unit (CAN-bus 2).

The research receives funding from the European Community Seventh Framework Programme (FP7/2007-2013) under grant agreement No 284078

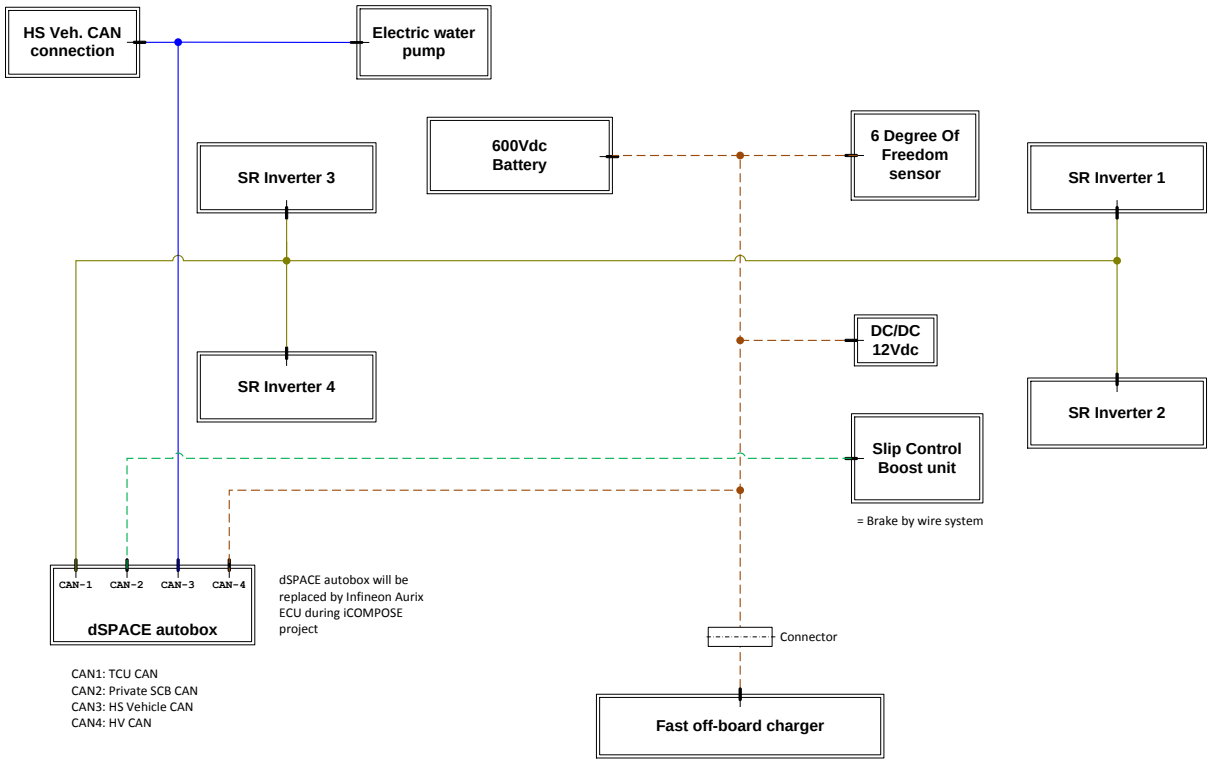

Figure 2.4.2.1 - Communication overview

All CAN-bus lines have the same baud rate of 500 kbit/s. The physical layer consists of CAN high, CAN low and GND. The base frame format and CAN 2.0 are used.

Flanders' DRIVE has investigated, in the scope of E-VECTOORC, the conversion of the communication over CAN with the MGU and TCU's to communicate via FLEXRay. This allows the system to communicate on a 1 ms time base due to the higher baud rate. The important advantages of FLEXRay are: dual bus as a physical layer, allowing for redundancy as well as the deterministic character, and message arrival information. The deterministic character is the most important because the bus is used for a safety critical application such as regenerative braking. The FLEXRay bus has been successfully tested in an experimental setup, including two functional TCU's, two listening TCU, the MGU and an analysis tool on a dual bus channel Figure 2.4.2.2. The tests were performed with a dummy car on the roller bench and the dual layer property (redundancy) was tested while controlling the motor torque. The performed test consisted of the interruption of one channel, while the other channel kept controlling the motor.

The research receives funding from the European Community Seventh Framework Programme (FP7/2007-2013) under grant agreement No.284078

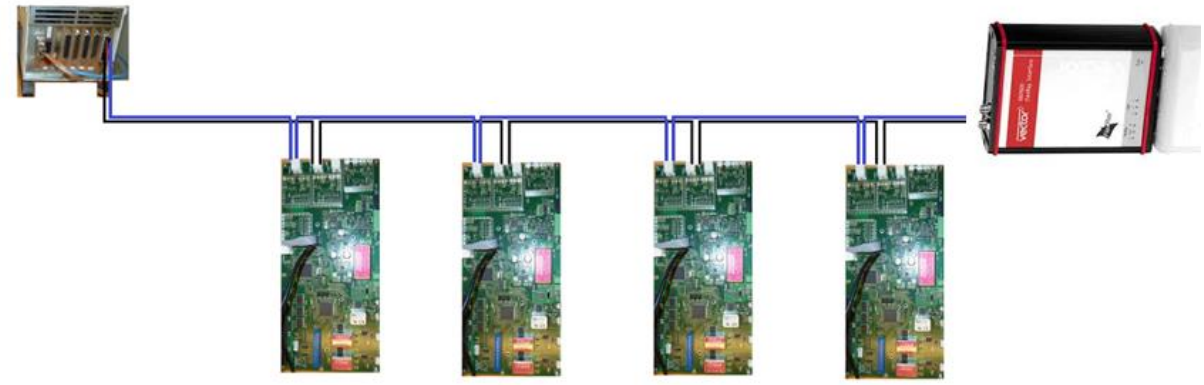

Figure 2.4.2.2 - Experimental dual channel FLEXRay layout including 4 TCU's, MGU and analysis tool.

2.5 Traction System Performance

2.5.1 Switched Reluctance Motor and Inverter

The vehicle demonstrator is actuated by 4 independent Switched Reluctance (SR) traction units consisting of the SR motor (SRM) and an accompanying Torque Control Unit (TCU). For integration the units are split in front and rear traction units comprising 2 motors and gear boxes similar to those shown in figures 2.5.1.1 and 2.5.1.2.

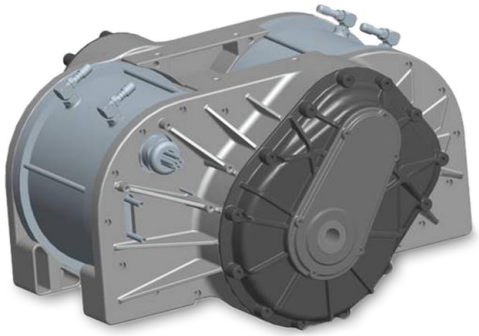

Figure 2.5.1.1 - Dual traction unit comprising two SRMs and two gearboxes

The research receives funding from the European Community Seventh Framework Programme (FP7/2007-2013) under grant agreement No 284078

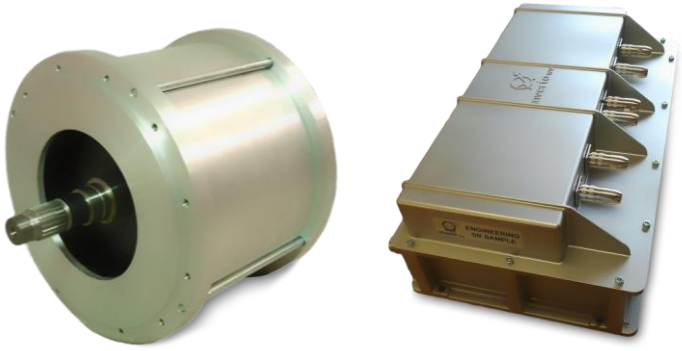

Figure 2.5.1.2 - SRM and TCU

The SR traction unit is designed for 800 V +/- 10% and outputs 100 kW peak power under this condition. As the vehicle demonstrator supplies 600 V the installed peak power reduces to 75kW.

The basic performance figures are mapped below in Figures 2.5.1.3 and 2.5.1.4 and Table 2.5.1.1. System efficiency is related to torque, speed and temperature. The performance in motoring and generating quadrant is very similar.

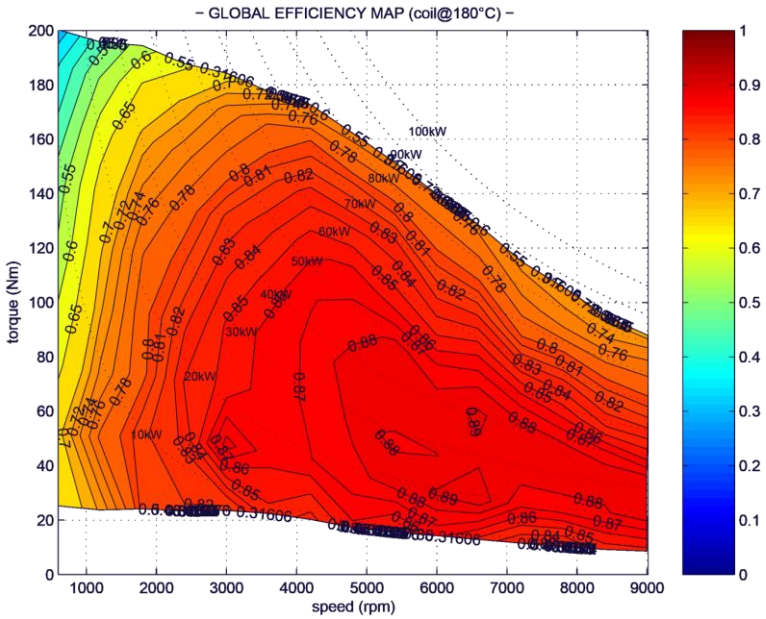

Figure 2.5.1.3 - Efficiency map in motoring quadrant @550V

The research receives funding from the European Community Seventh Framework Programme (FP7/2007-2013) under grant agreement No 284078

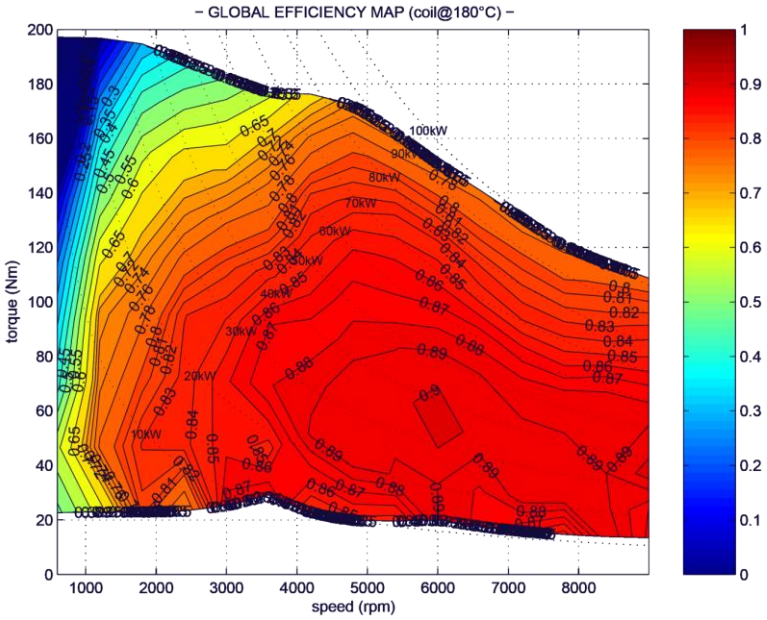

Figure 2.5.1.4 - Efficiency map in generating quadrant @550V

Table 2.5.1.1 - Motor Characteristics

TORQUE/POWER @ 600 V	
Peak (30 s)	200 Nm, 75 kW
Nominal (continuous)	80 Nm, 35 kW
Maximum speed	14000 rev/min
Motor dimensions (L x D)	215 x 265 mm
Motor mass	50 kg
Motor inertia (without gearbox)	21087 kgmm²
Inverter dimensions (W x H x D)	495 x 155 x 282 mm
Inverter mass	16.2 kg
Liquid cooled	15 l/min, 55°C max inlet
Operating temperature	-40 – 85°C

2.5.2 Battery pack

The battery pack is designed as a power pack so that the maximum allowed amount of power for charging and discharging is the same. The details of the battery pack are given in Table 2.5.2.1. In order to allow quick assembly and testing of the vehicle demonstrator, a lower power (400 V) pack was used during the initial stages of the project.

Table 2.5.2.1 - Battery Pack Specifications

Pack nominal voltage	600 V
Pack maximum voltage	772.8 V
Pack minimum voltage	414 V
Peak current charge and discharge	400 A
Nominal current (continuous) charge and discharge	200 A

The research receives funding from the European Community Seventh Framework Programme (FP7/2007-2013) under grant agreement No 284078

Peak power charge and discharge	310 kW
Nominal power charge and discharge	121 kW
Cell capacity	15 Ah
Energy	9.1 kWh
Mass	~300 kg (225 kg for 400V pack)
Operating temperature	0 – 55°C

The 600 V battery pack can handle 400A peak current for a limited time. Figures 2.5.2.1 and 2.5.2.2 show the relation between the absolute nominal and peak current. When the nominal current is low, more peak current pulses can be handled by the battery pack. When the nominal current is high the time between the allowed peak current pulses is longer. With a low nominal current the frequency of the peak current is higher, the wait time shorter. A high nominal current gives a lower frequency. The duration of the peak currents is in both cases 10 seconds. The root mean square of the current from the battery pack must be kept below 200 A and the peak current is limited to 400 A for 10 seconds.

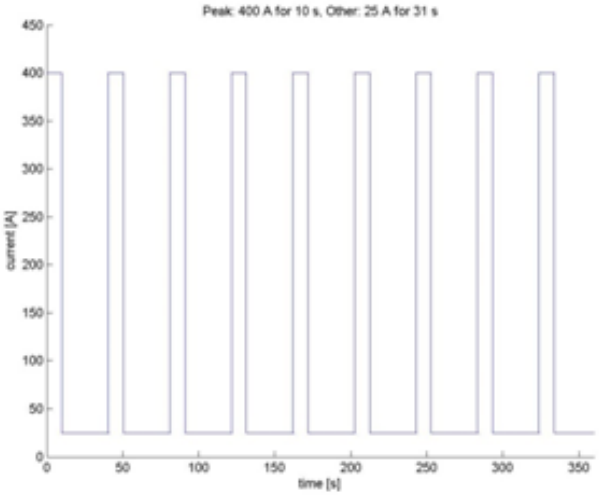

Figure 2.5.2.1 - Frequency of allowed 400 A current peaks for low nominal current condition (25 A)

The research receives funding from the European Community Seventh Framework Programme (FP7/2007-2013) under grant agreement No 284078

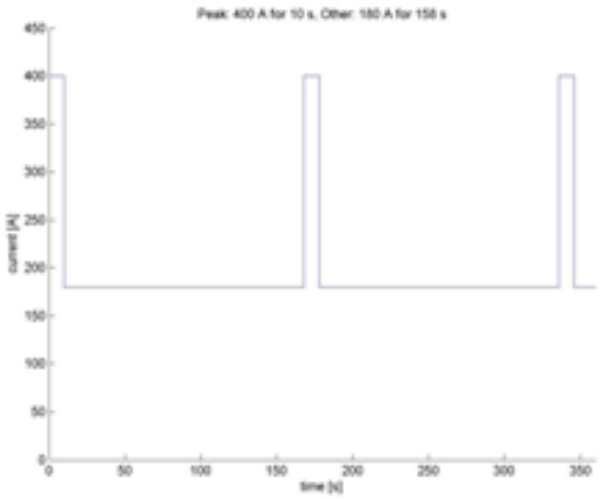

Figure 2.5.2.2 - Frequency of allowed 400 A current peaks for high nominal current conditions (180 A)

2.5.3 Off-board charger specifications

The off-board fast charger is connected with a high voltage connector to the high voltage distribution box. The specifications of the off-board fast charger are given in Table 2.5.3.1.

Table 2.5.3.1 – Off-board charger specifications

INPUT DATA	
Input voltage range	185-276 Vac
Line frequency	47-63 Hz
Input current	96 A (AC) @ 185Vac
Absorbed maximum apparent power	22.3 kVA
Power factor	>0.98/
OUTPUT DATA	
Charging voltage range	300-800 V (DC)
Voltage accuracy	±1%
Output current max	25 A (DC)
Rated output power	20 kW
GENERAL	
Cooling	Liquid
Mass	65 kg

2.5.4 Energy Management

The motor generator control unit (MGU) decides where the power comes from or goes to. These algorithms are based on the inputs coming from the BMS, SR-motors and inverters, and the driver demand.

Primarily, the current protection is managed in the BMS since all the cell voltages and the current flowing through the battery pack are monitored here. Based on these measurements

The research receives funding from the European Community Seventh Framework Programme (FP7/2007-2013) under grant agreement No 284078

the BMS sets the limits for the battery pack. This is communicated via CAN to the MGU. Based on the inputs from the BMS, the energy coordinator set the current limit towards the charger and the torque distributor sets the regenerative and motoring torque limits towards the switched reluctance inverters.

2.6 Braking System

The friction brake system implemented in the E-VECTOORC concept is being developed on the basis of the second generation of Slip Control Boost (SCB) system by the project partner TRW. Figure 2.6.1 shows the SCB integrated in the E-VECTOORC architecture.

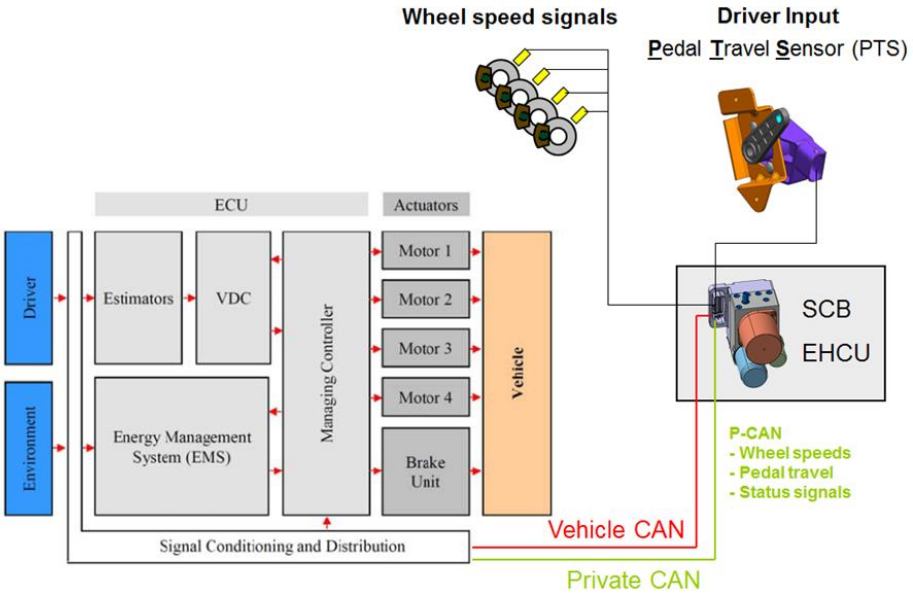

Figure 2.6.1– Architecture of SCB system

The SCB system is coupled to other vehicle subsystems and components through two CAN connections. The conventional CAN enables embedding the SCB system into the vehicle architecture. The private CAN is mainly used for status signals as well as pedal travel and wheel speed signals.

As part of the E-VECTOORC brake system, the SCB-unit is normally managed by the E-VECTOORC vehicle control unit (VCU) implemented on the dSpace MicroAutoBox. This takes the driver braking request via the pedal travel transmitted by the SCB unit via CAN, calculates the total braking torque required to achieve the desired deceleration, and

The research receives funding from the European Community Seventh Framework Programme (FP7/2007-2013) under grant agreement No 284078

apportions the torque to the e-motors or friction brakes; in the latter case by issuing semi-autonomous pressure demands to the SCB. These demands can be “regular” pressure demands for front and rear axles under base brake conditions or demands for individual pressure control on specific wheels for ESC-type interventions or torque vectoring events.

If a problem exists within the VCU, it is possible that the driver demand for braking is not acted upon, so several fault detection methods are used that cause the brake system to revert to working entirely within the SCB unit – in a so-called ‘failed (or internal) mode”. Thereby the SCB fulfils the task of providing a safe backup brake system.

Within these two basic operating regimes (external control / internal control) different control modes of the SCB unit are activated. The specific functions are explained in detail in section 2.6.3.

2.6.1 Components of the SCB system

The SCB configuration in the E-VECTOORC project is characterised by more compact mass and dimensional parameters as compared with the competitive x-by-wire brake systems. In particular, the mass of the master cylinder is 2.5 kg without the brake fluid reservoir. The mass of the electro-hydraulic control unit with 120 cc accumulator is about 8.1 kg. Figure 2.6.1.1 shows the design of relevant components.

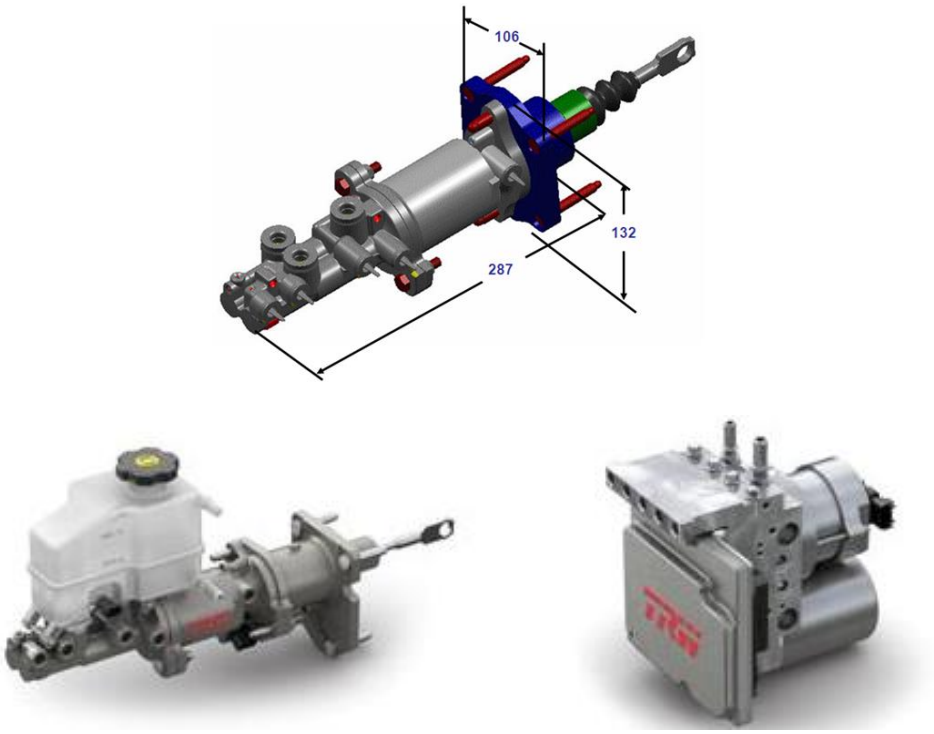

Figure 2.6.1.1 –The SCB components: master cylinder; electro-hydraulic control unit

The research receives funding from the European Community Seventh Framework Programme (FP7/2007-2013) under grant agreement No 284078

The SCB has a decoupled configuration, i.e., the brake system has an embedded travel simulator. For this purpose, the brake pedal unit contains a travel sensor providing the information for further definition of brake torque (motor torque or pressure) demand. The mounting of the travel sensor is shown in Figure 2.6.1.2.

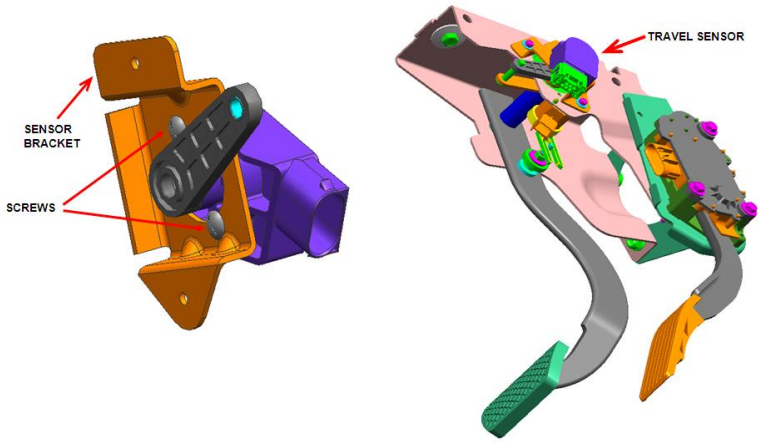

Figure 2.6.1.2– Mounting of the travel sensor

The travel sensor used in the SCB is the BPS Contactless Inductive Position Sensor produced by Hella as shown in Figure 2.6.1.3. The operation of the sensor is as follows. A printed winding on a PCB element is powered with an AC current. A ferromagnetic target (Rotor) is used as a magnetic core. Depending on the position of the core an AC current of some MHz is inducted into two printed windings on the PCB. These two windings are phase shifted by 90°. As a result a sinus and co-sinus signal is generated. Changing the position of the Rotor relative to the printed winding on the PCB will change the amplitude of the induced voltage. The Rotor has to be located close to the PCB; between the rotor and the PCB only air or plastic parts are allowed.

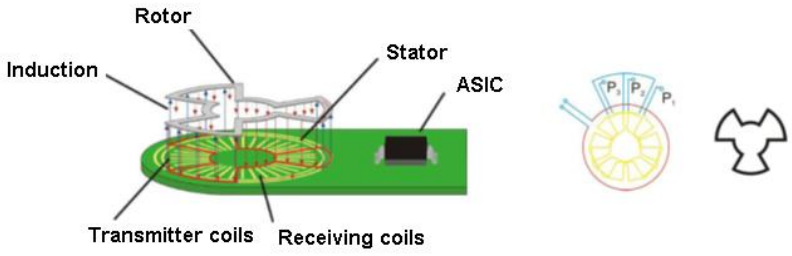

Figure 2.6.1.3 – Travel sensor construction

The research receives funding from the European Community Seventh Framework Programme (FP7/2007-2013) under grant agreement No 284078

2.6.2 Commissioning of the SCB system

A cascaded testing process has been established, starting with tests on various test rigs - with increasing complexity of the test cases - and ending with release tests in the vehicle.

1. First stage: standard open-loop tests of the SCB-system to check basic functionality (mainly the base brake tests).
2. Second stage: Extend the tests from first stage using generic input data for the braking controller (e.g. wheel speeds) and operate the system in closed-loop conditions but stand-alone to check the basic control capabilities (ABS/TC/VSC).
3. Third stage: Integration of the SCB-system into a vehicle environment and verification of the tests from the second stage in a more complex and dynamic situation, mainly with respect to the communication between different protocols, controllers and functions. Focus of these tests is the fault free operation of all control functions and the evaluation of the fail-safe strategies in case of errors.
4. Fourth stage: Evaluation of the performance of all control functions in a vehicle environment.

2.6.3 Control modes of the SCB unit

Figure 2.6.3.1 shows the different operating modes of the SCB unit, which are explained in more detail further below

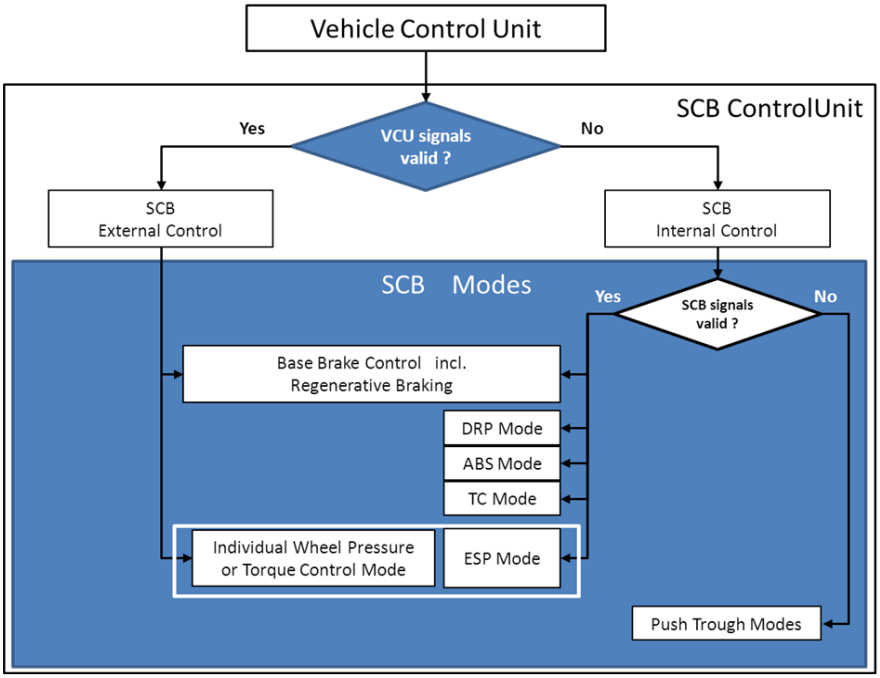

Figure 2.6.3.1 - Operating regimes of the SCB unit and activated functions

The research receives funding from the European Community Seventh Framework Programme (FP7/2007-2013) under grant agreement No 284078

SCB Base Brake Control Including Regenerative Braking

The sequence of events during a base braking scenario with all systems functioning and the High Pressure Accumulator (HPA) charged to a pressure between 140 and 180 bar is shown in Figure 2.6.3.2

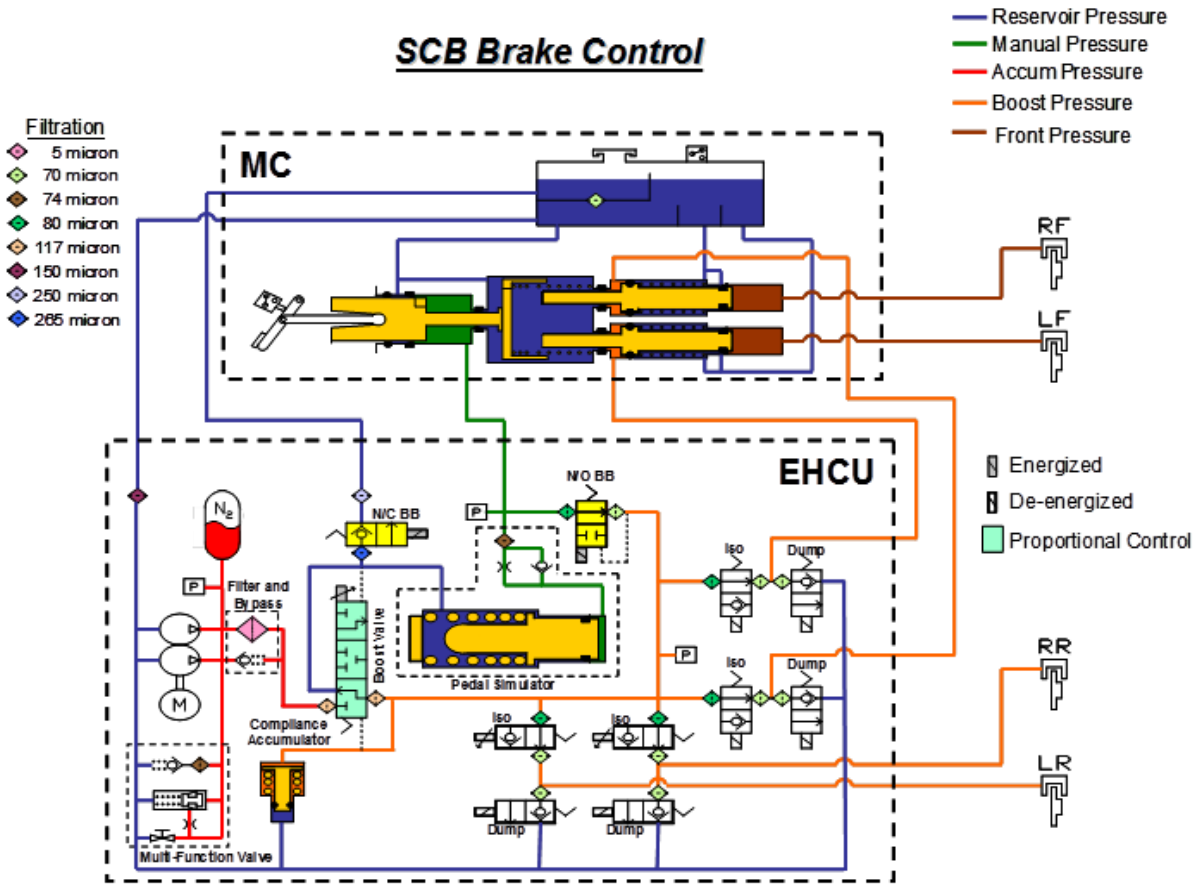

Figure 2.6.3.2 – SCB base brake control mode

The driver's braking demand is measured by the travel sensor and the pressure sensor before the Normally Open Base Brake (N/O BB) valve. These sensors are the inputs to the base brake control algorithm which determines the brake pressure in the system during normal operation.

The N/O BB, Normally Closed Base Brake (N/C BB), and boost valves are activated at the onset of brake control. Pressure in the master cylinder (MC) primary circuit, resulting from the pedal simulator movement, provides the driver's force feedback during normal base and regenerative braking. The Pedal Simulator is interchangeable and can be designed to provide varying degrees of pedal feel for a specific vehicle application.

The research receives funding from the European Community Seventh Framework Programme (FP7/2007-2013) under grant agreement No 284078

The boost valve proportionally controls the fluid from the HPA to increase the brake pressure or reduces it by returning fluid to the reservoir. The brake pressure is constantly modulated based on the pressure control algorithm.

SCB Control during Dynamic Rear Proportioning (DPR) Mode

The sequence of events during a base braking scenario with no regenerative braking with the HPA charged to a pressure between 140 and 180 bar is shown in Figure 2.6.3.3

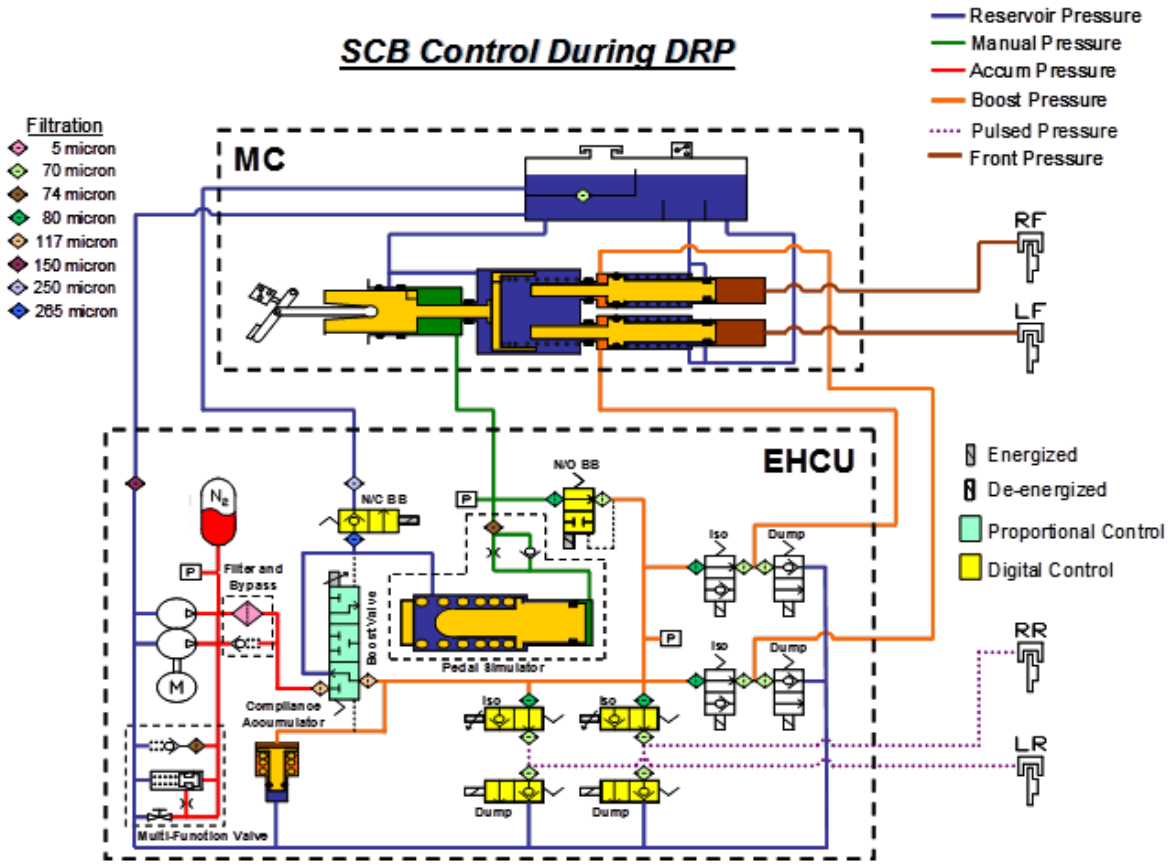

Figure 2.6.3.3 – SCB DRP control mode

Driver intent braking is controlled in the same way as in the Base Braking described above. The pressure in the rear brakes is digitally controlled using the isolation (iso) and dump valves to provide adequate front to rear brake proportioning.

The research receives funding from the European Community Seventh Framework Programme (FP7/2007-2013) under grant agreement No 284078

SCB Control during ABS Mode

The sequence of events when wheel slipping is detected on all four wheels with the HPA charged to a pressure between 140 and 180 bar is shown in Figure 2.6.3.4.

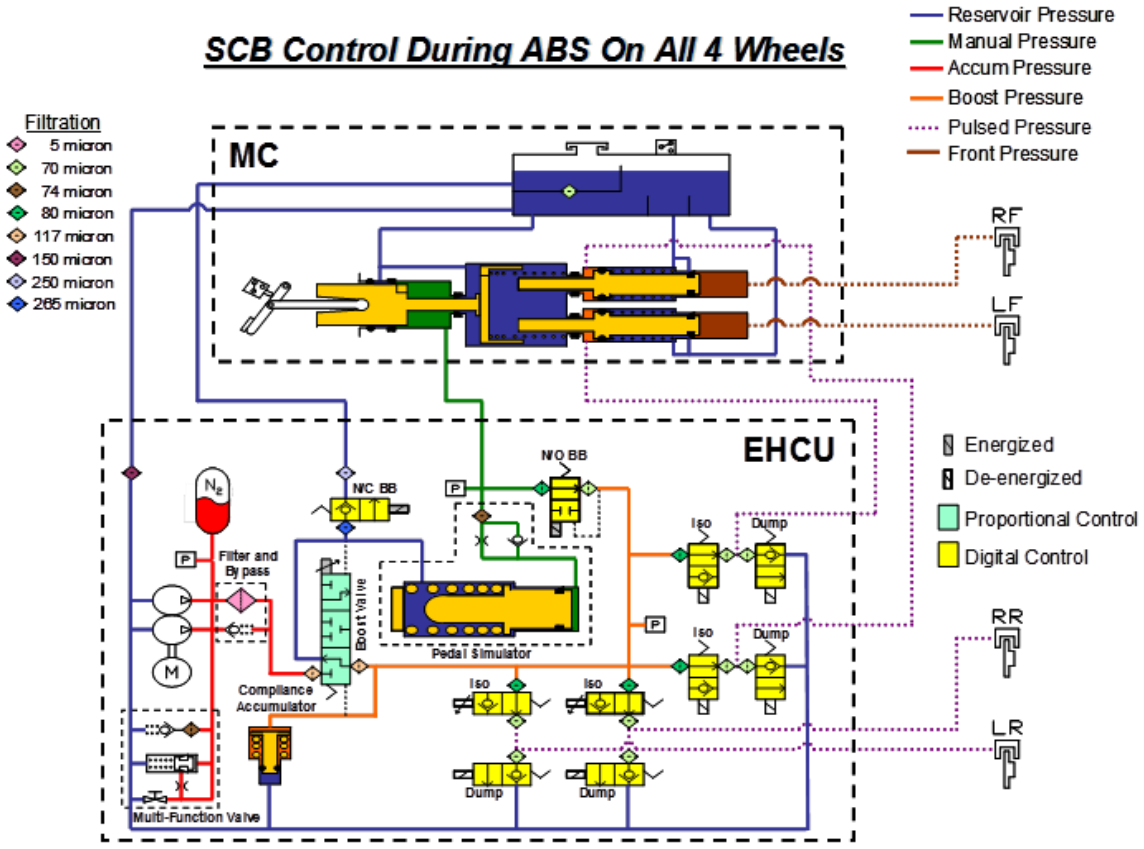

Figure 2.6.3.4 – SCB ABS control mode

Driver intent braking is controlled the same way as in the base braking described above.

Four iso valves are energized to isolate the boost valve pressure from the brakes when the wheel slipping is detected on all four wheels. The compliance accumulator provides the necessary displacement to the boost valve to prevent unnecessary pressure feedback because of the dead headed hydraulic circuit when all the iso valves are simultaneously energised.

The iso and dump valves are digitally controlled to modulate the pressure in the brakes for the required wheel slip level.

The research receives funding from the European Community Seventh Framework Programme (FP7/2007-2013) under grant agreement No 284078

SCB Control during ESC Mode – Individual Wheel Pressure/Torque Control

Figure 2.6.3.5 shows the sequence of events when the Electronic Stability Control (ESC) control algorithm determines the case of additional braking on the right wheels, during a braking event, with the HPA charged to a pressure between 140 and 180 bar.

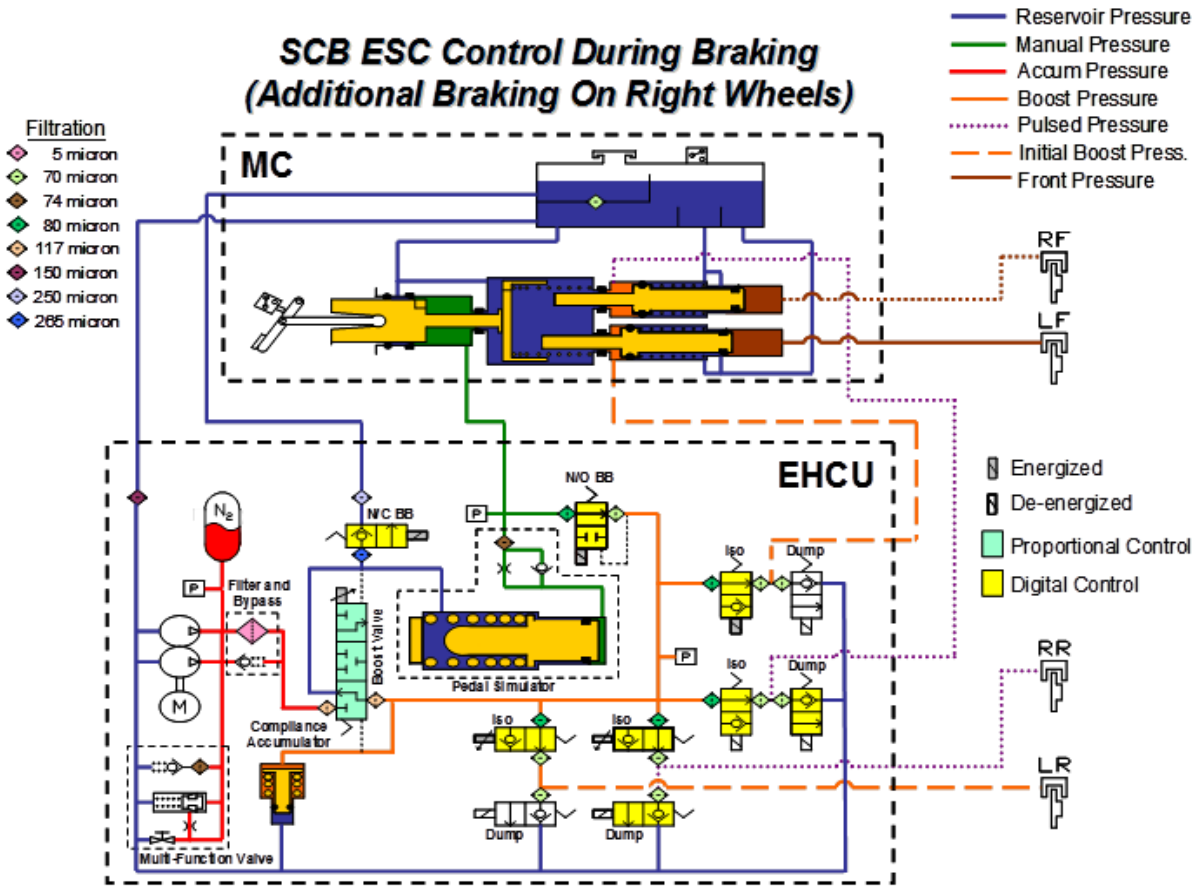

Figure 2.6.3.5 – SCB ESC control mode

Driver intent braking is controlled the same way as in the base braking described above. When an ESC manoeuvre is detected and additional braking is required on the right wheels, the iso valves are energised to isolate the boost valve pressure from the four brakes. The boost valve will then increase the pressure before the iso valves to a level greater than originally commanded. The RF and RR iso valves will then be digitally controlled to provide additional pressure to the right wheels as required by the ESC control algorithm.

The same procedure is used for individual wheel pressure control. In this case the iso valves are digitally, but independently controlled to provide the requested pressure (form the VCU) at the specific wheels. To achieve the necessary accuracy the algorithm uses the known

The research receives funding from the European Community Seventh Framework Programme (FP7/2007-2013) under grant agreement No 284078

(internally measured) system pressure before the iso valves, their flow characteristic and the calibrated calliper stiffness to estimate the opening time until the required wheel pressure is reached. Extensive tests executed on HIL rigs as well as in the vehicle have shown the very good reproducibility and correlation (between requested and achieved wheel pressure) of this approach.

SCB Control during Right Rear Wheel TC Intervention

Figure 2.6.3.6 presents the sequence of events when the TC control algorithm determines the right rear wheel requires braking with the HPA charged to a pressure between 140 and 180 bar.

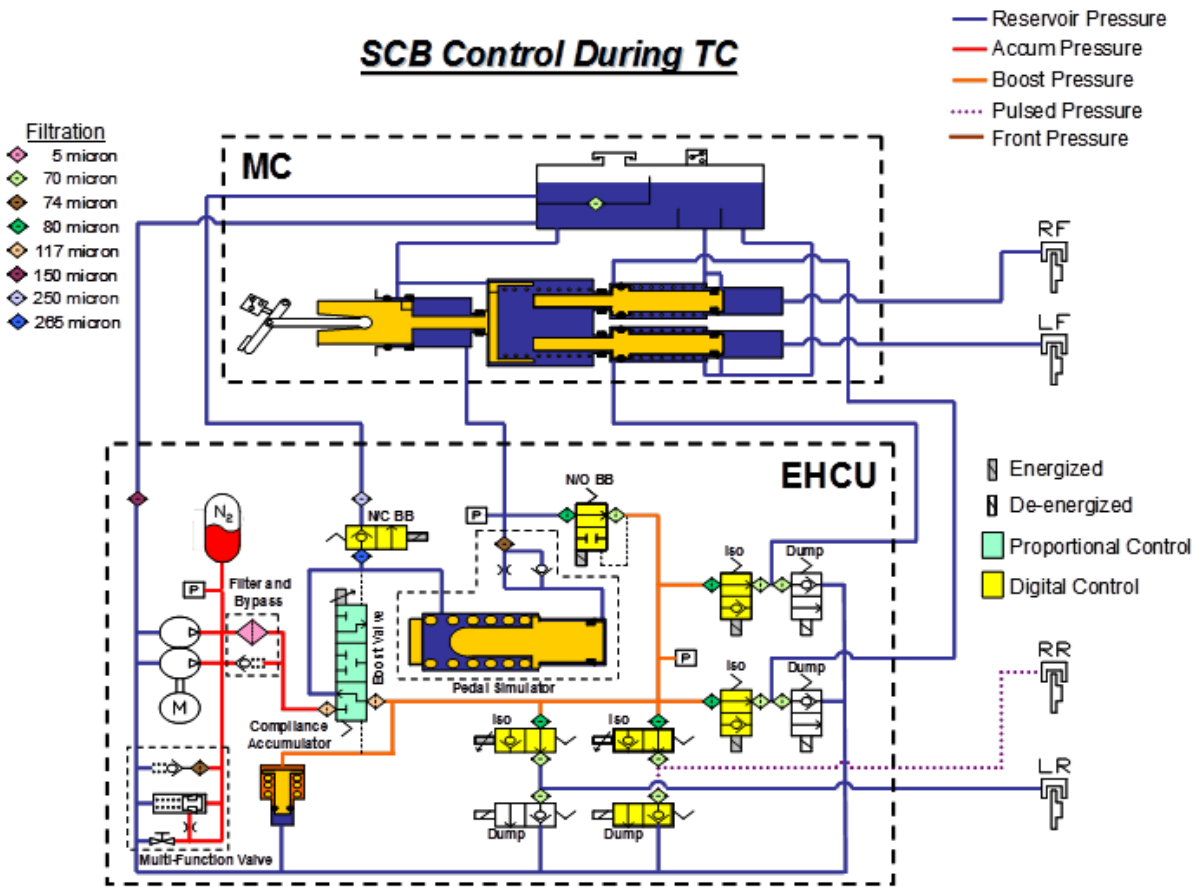

Figure 2.6.3.6 – SCB control mode by traction control intervention

The N/O BB, N/C BB, and all the iso valves are energised. The boost valve then proportionally controls the pressure, before the iso valves, to a value determined by the TC

The research receives funding from the European Community Seventh Framework Programme (FP7/2007-2013) under grant agreement No 284078

control algorithm. The RR iso and dump valves are digitally controlled to provide the brake pressure that regains the necessary traction.

SCB Control during 4 Wheel Push Through

Figure 2.6.3.7 shows what occurs when the SCB EHCU is not functioning due to some failure detection.

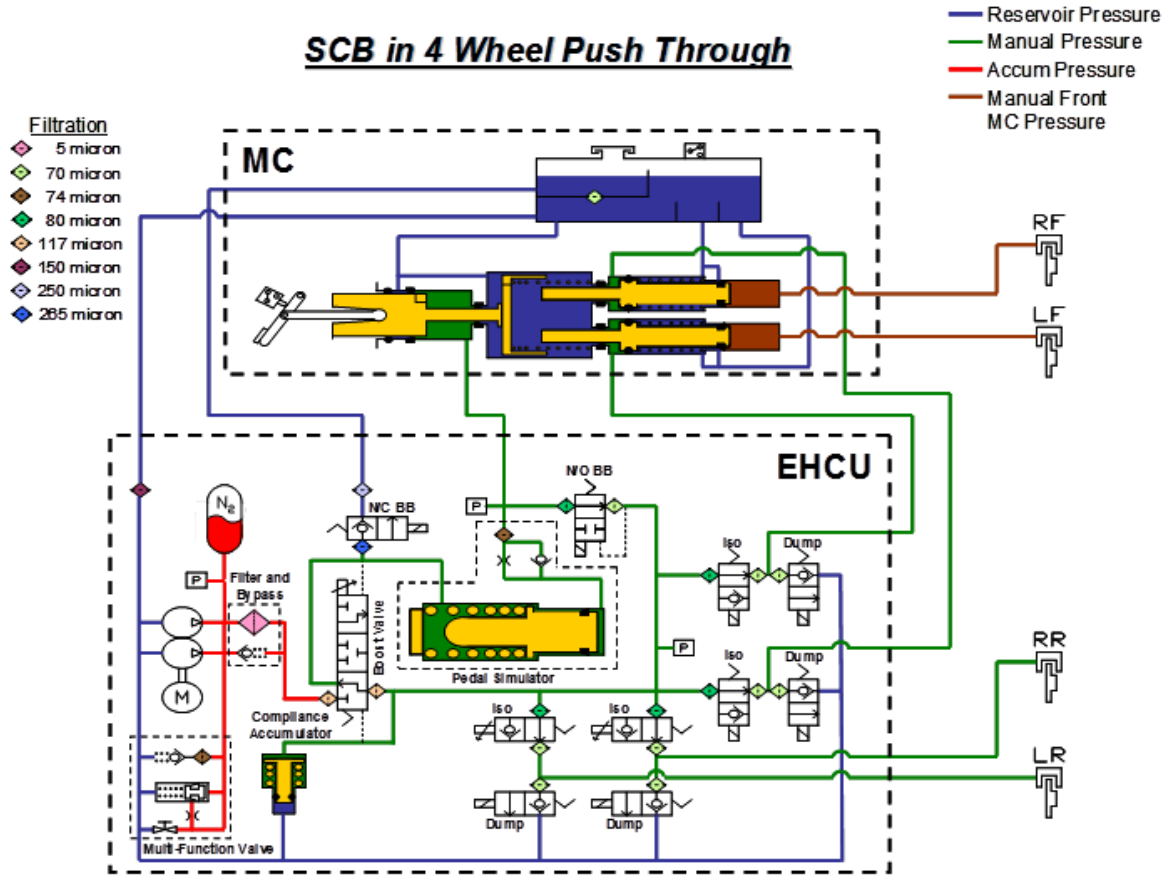

Figure 2.6.3.7 – SCB control mode by 4 wheel push through

The driver pushes on the brake pedal, which generates pressure in the brakes from the MC primary circuit. The Pedal Simulator cannot move because it is hydraulically locked due to the N/C BB valve being de-energised. The fluid flow from the spring chamber of the pedal simulator to the reservoir cannot occur in this state.

The research receives funding from the European Community Seventh Framework Programme (FP7/2007-2013) under grant agreement No 284078

SCB Control during 2 Wheel Push Through

Figure 2.6.3.8 depicts what occurs when the SCB system detects a failure in the Primary MC circuit and the system is not functioning.

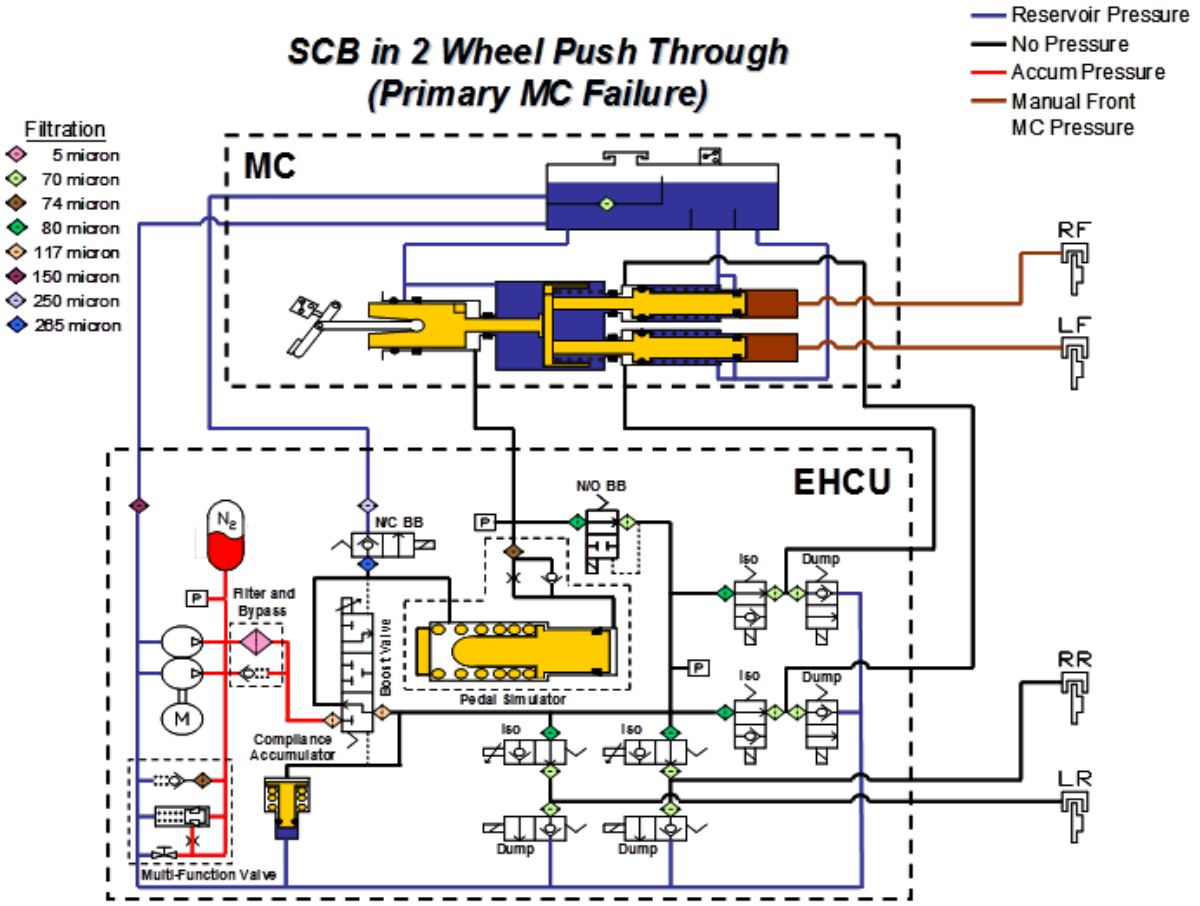

Figure 2.6.3.8 – SCB control mode by 2 wheel push through

The driver pushes on the brake pedal, which generates pressure in the front brakes from the MC secondary circuits. The brake pedal movement results in the primary piston having direct mechanical force translation to the MC secondary pistons. No pressure will be generated in the rear brakes.

The research receives funding from the European Community Seventh Framework Programme (FP7/2007-2013) under grant agreement No 284078

2.7 Cooling System

The vehicle is equipped with a liquid cooling system for controlling the temperature of the switched reluctance motors and inverters. The cooling architecture is presented in Figure 2.7.1. The flow of the pump is adjustable via CAN. The battery is forced air cooled.

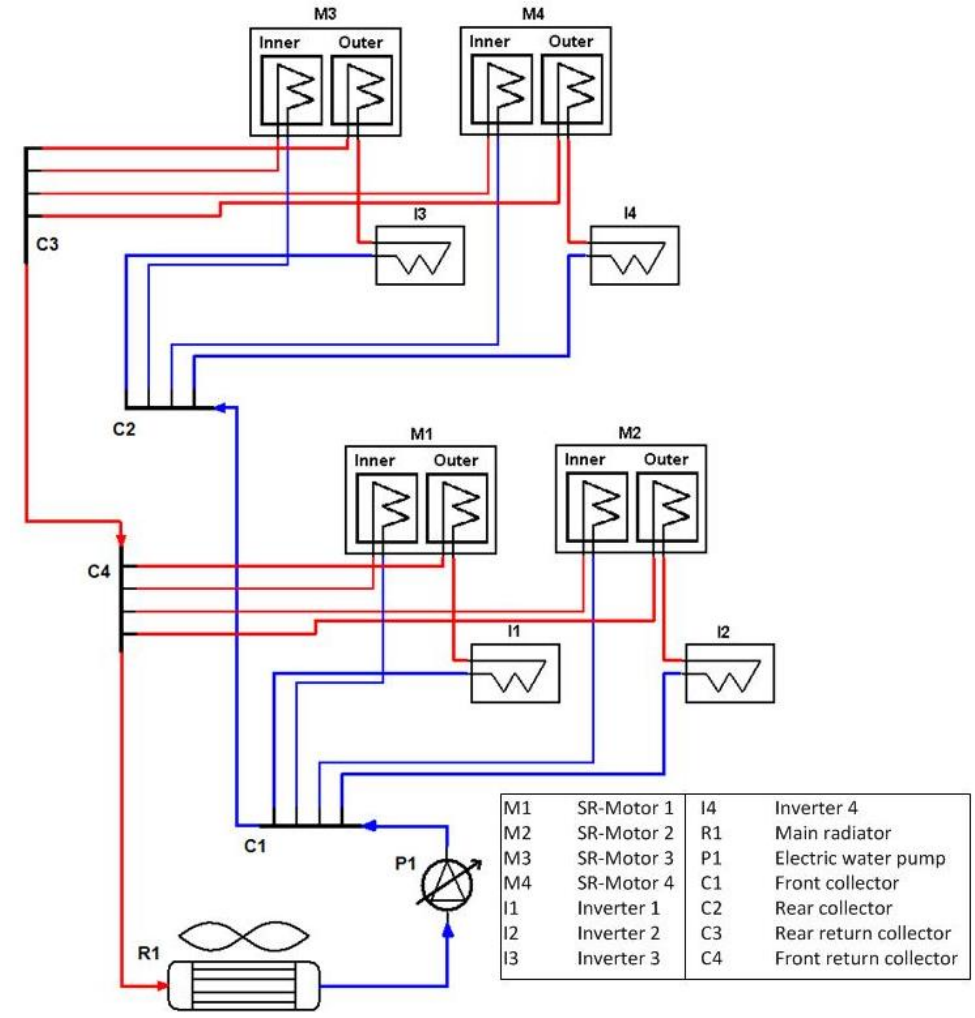

Figure 2.7.1: Cooling architecture

The 12 Vdc converter is not drawn in Figure 2.7.1, but it is liquid cooled and connected to the front collector and front return collector. The 12 Vdc converter cooling circuit has a pressure drop of 0.1 bar @ 4 l/min. The size of the radiator is 670 mm x 449 mm x 26 mm. The entire cooling circuit is filled with a coolant existing of 50% of water and 50% of glycerol. Each SR-motor has two cooling circuits, an inner and outer jacket. The SR-inverter has one cooling jacket. The warm coolant from the inverters flows through the outer jacket of the motor and

The research receives funding from the European Community Seventh Framework Programme (FP7/2007-2013) under grant agreement No 284078

returns to the radiator. The coolant specifications for the SR drive are 15 l/min and a maximum inlet temperature of 55°C.

As the vehicle is designed as a demonstrator/experimental vehicle the original air conditioning was removed from the car.

2.8 Measurement and Control Instrumentation

2.8.1 Corrsys-Datron

A CORREVIT® S-350 Aqua non-contact 2-axis optical sensor (Figure 2.8.1.1) is fitted to the vehicle to provide signals relating to the velocity vector over ground. The performance is described in table 2.8.1.1 below.

Figure 2.8.1.1 CORREVIT® S-350 Aqua non-contact 2-axis Optical Sensor

Table 1.8.1.1 - CORREVIT® S-350 Aqua non-contact 2-axis Optical Sensor Performance Specifications

Performance specifications		
Speed range:	0.5 ... 250	Km/h
Distance resolution:	2.47	mm
Distance measurement deviation:	<±0.2	%
Angle range:	±40	degrees
Angle resolution:	<±0.1	degrees
Update rate	250	Hz

The research receives funding from the European Community Seventh Framework Programme (FP7/2007-2013) under grant agreement No 284078

2.8.2 6 – DOF Accelerometer

The accelerometer is the conventional 6 degree of freedom inertial sensor (Figure 2.8.2.1) installed on the Range Rover Evoque. This unit is read over CAN into the dSpace unit.

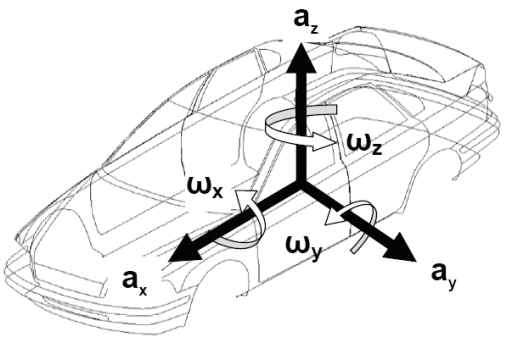

Figure 2.8.2.1 - Six degrees of freedom measured by the accelerometer (IMU)

2.8.3 Wheel Speed Signals

Wheel speed signals are the intelligent sensors used on the Range Rover Evoque (Table 2.8.3.1), read by the TRW SCB system in conventional manner. Whilst those on the rear wheels are intelligent and provide one pulse for each edge of the toothed wheel, those on the front describe only the profile of the teeth. Edge detection in the dSpace unit makes the two types functionally similar.

Table 2.8.3.1 - Wheel Speed Pulses per revolution

Wheel Speed Sensors	Tone Wheel	Electrical Signal
Front Wheels	48 teeth	48 pulses per revolution
Rear Wheels	46 teeth	92 pulses per revolution

The research receives funding from the European Community Seventh Framework Programme (FP7/2007-2013) under grant agreement No 284078

2.8.4 Torque Measuring Wheels

For the purposes of direct dynamic measurement of wheel forces (in longitudinal, lateral and vertical directions) and wheel moments (in pitch, roll and yaw planes), the vehicle demonstrator is instrumented with the wheel force sensor RoaDyn S635 produced by Kistler. The sensor, as shown in Figure 2.8.4.1, has the performance data listed in Table 2.8.3.2.

Table 2.8.3.2 - Wheel force sensor performance data

Measuring range	
Fx	–35 ... 35 kN
Fy	–20 ... 20 kN
Fz	–35 ... 35 kN
Mx	–5 ... 5 kNm
My	–5 ... 5 kNm
Mz	–5 ... 5 kNm
Rotary angle accuracy	≈0,1 degrees

Accuracy	
Crosstalk	
Fy –> Fx, Fz	≤1%
Fx <–> Fz	≤1%
Fx, Fz –> Fy	≤2%
Linearity	≤0.5% v.E
Hysteresis	≤0.5% v.E
Maximum speed	2 300 rpm (≈280 km/h)

Figure 2.8.4.1 The Kistler wheel sensors

2.8.5 Steering Robot

A steering robot is installed to allow repeatable vehicle dynamics control studies to be executed. These apply accurate, controlled inputs to a vehicle's steering system as required for a wide range of tests including for transient handling behaviour such as fishhook, sine-dwell and step steering. They enable a wide range of steering inputs to be applied with high precision and repeatability to enable high quality data to be gathered quickly

The Anthony Best dynamics SR60 robot has been installed. The specifications for this are given in Table 2.8.5.1.

The research receives funding from the European Community Seventh Framework Programme (FP7/2007-2013) under grant agreement No 284078

Table 2.8.5.1 - Steering Robot Specifications

Maximum Torque	70 Nm at 580 deg/s
Rated Torque	60 Nm at 1300 deg/s
Maximum speed	2500 deg/s at up to 10Nm
Motor Mass	12.5 kg

2.8.6 dSpace

The dSpace installation is a MicroAutoBox as widely used for rapid prototyping of vehicle dynamics experimentation.

Figure 1.8.6.1 - dSpace MicroAutoBox

3 Performance of the Electric Motors

Previous deliverables have described the motor specifications/design and performance test results are presented elsewhere. This section discusses some of the issues relating to the installation of the motors.

During commissioning, issues associated with the performance of the electric motor consisted of:

1. The consequence of the supply voltage
2. Mechanical issues with the position resolver and with the motor rotors
3. The communications channels
4. Torsional vibrations in the driveshafts as the car moved off, the torque ripple from the motors was suspected and to help with this a modification to the contol software was implemented to reduce the torque ripple.
5. Torque estimation for the vehicle control was analysed in depth and algorithms were developed to improve this.
6. Thermal charateristics of the motors were extensively analysed and a real time model implemented so as to allow higher transient performance.

The research receives funding from the European Community Seventh Framework Programme (FP7/2007-2013) under grant agreement No 284078

These issues are reported in detail in the following sections.

3.1 Effect of battery voltage

The original design specification was set to 800 V (+/-10%). The voltage relates directly to the power capability of the motor and is a major design issue as it appoints for the current rate of the converter and the winding design of the machine.

The peak power requirement of 100 kW is met at the minimum voltage of 720V, which is the expected voltage drop of the battery system under full load (minus 10%). For higher potentials 100 kW is not a problem.

3.1.1 400 V battery pack

In an initial stage, Flanders' Drive used a 400 V battery system to power the motors. This lowers the Volt-Ampère availability by a factor of 2 and also reduces the peak power consequently by 2 resulting in 50 kW peak power instead of 100 kW.

The optimized torque map at 800 V is affected when operating at 400 V and results in a discontinuous torque relation at higher speed. New control optimisation was carried out to overcome this problem. The torque map was not validated on the test bench, but only evaluated by the vehicle performance.

At lower voltage additional motor losses will appear, resulting in a thermal derating of the machine in the higher power region. This is explained by the flux current relation:

$$T = \Psi \times i = \int u dt \times i$$

The current should also be doubled for the same power at half potential resulting in an increase in copper losses by of factor 4. A loss comparison between 800 V and 400 V is included in Figure 3.1.1.1.

The research receives funding from the European Community Seventh Framework Programme (FP7/2007-2013) under grant agreement No 284078

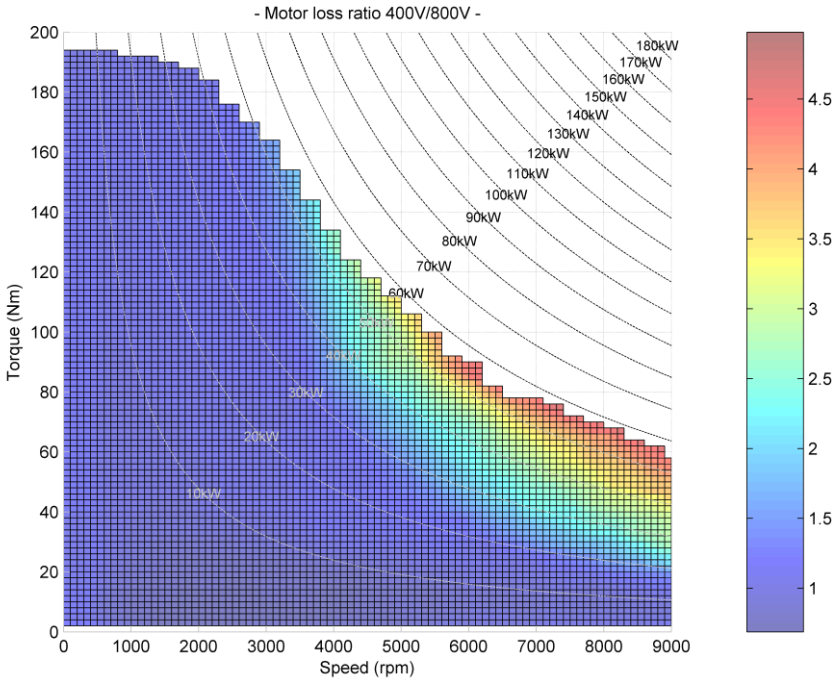

Figure 3.1.1.1 - Motor loss comparison 800 V versus 400 V

3.1.2 600 V battery pack

Flanders' Drive updated the vehicle with a 600 V battery pack in April 2014. This will reduce peak power by only a factor of 600/800 and will end up with a peak power of 75 kW. New control parameters were optimized for 600 V. Also, additional losses are introduced at high power, nevertheless much smaller than at 400 V.

3.1.3 Thermal derating comparsison 800/600/400V

In Figure 3.1.3.1 the nominal torque/power lines are set based on simulated motor losses and the identified thermal model of the machine.

- @800 V 80 Nm / 35 kW nominal
- @600 V 80 Nm / 35 kW nominal
- @400 V 80 Nm / 25 kW nominal

This shows a similar thermal loading along peak lines for 600 and 800 V

The research receives funding from the European Community Seventh Framework Programme (FP7/2007-2013) under grant agreement No 284078

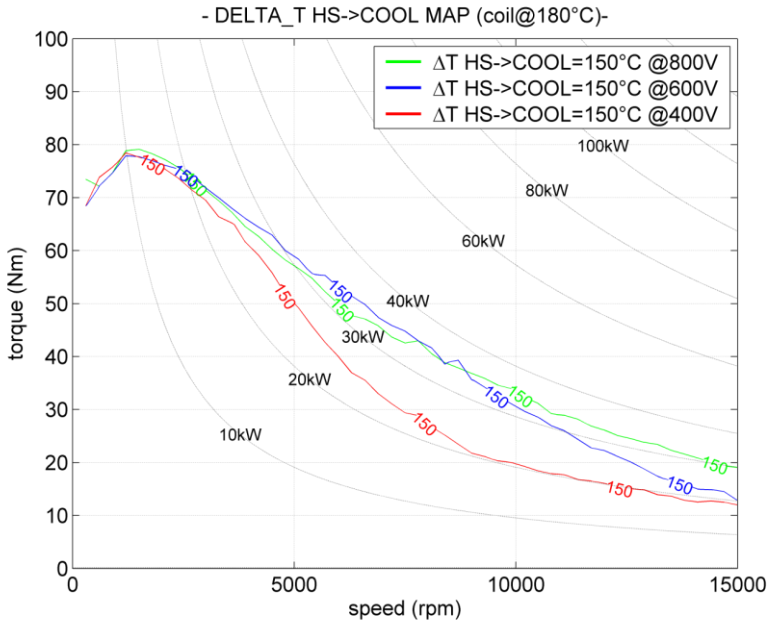

Figure 3.1.3.1 - Nominal power estimation for 800/600/400V

3.2 Motor/drive hardware updates

3.2.1 Resolver

An assembly issue was highlighted in the rotor axial position, which is fixed by the A-bearing in the gear box. Shims were needed to level the axial resolver position.

An 'Out of spec' hardware-error in the motor drive, was solved at first by hardware gain (+10%; +20%; +40%: ‘out of spec’ at any torque) then by mechanical disassembly of the motor/gear. 1.3-1.4mm axial displacement by faulty gear box spline nut was detected due to incorrect pretension.

The research receives funding from the European Community Seventh Framework Programme (FP7/2007-2013) under grant agreement No 284078

Figure 3.2.1.1 - Resolver

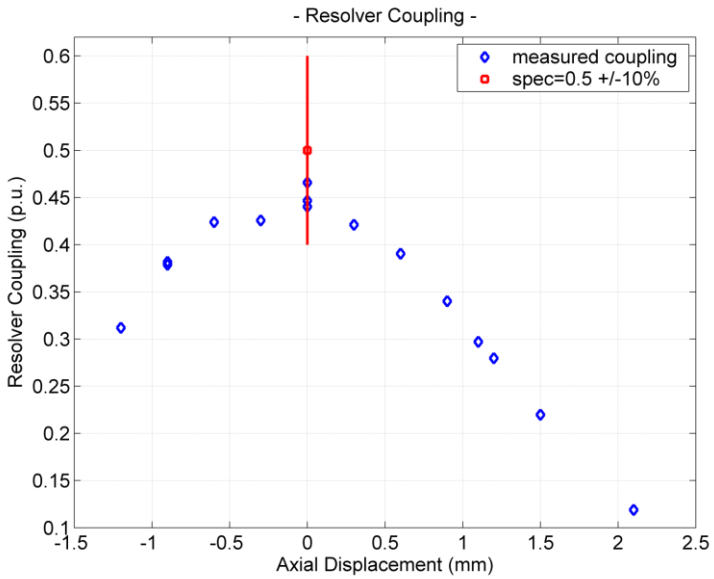

Figure 3.2.1.2 - Resolver coupling

3.2.2 Rotor shrouds

The production procedure is that the shrouds are shrunk onto the rotor shaft (>250°C), the shroud having similar thermal properties to the shaft.

Inductive power loss colouring revealed that local temperatures had exceeded approx. 350°C, implying about 500 W unexplained power loss against simulation. Without cooling, a temperature delta of 350°C is possible for 6 minutes with a 1.1kg total disc weight. The solution to the damaged rotors was to reduce the discs and weld them onto the shaft.

Four new rotors with improved material and shape were designed in Dec 2013 and installed in Jan 2014.

The research receives funding from the European Community Seventh Framework Programme (FP7/2007-2013) under grant agreement No 284078

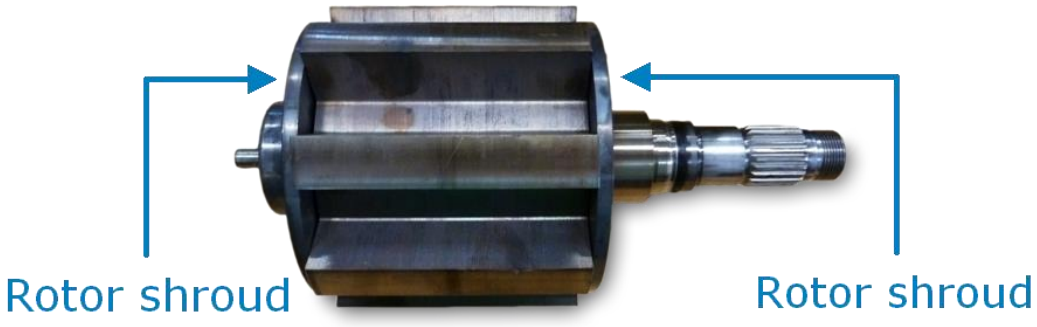

Figure 3.2.2.1 - First rotor design with potential loose rotor discs

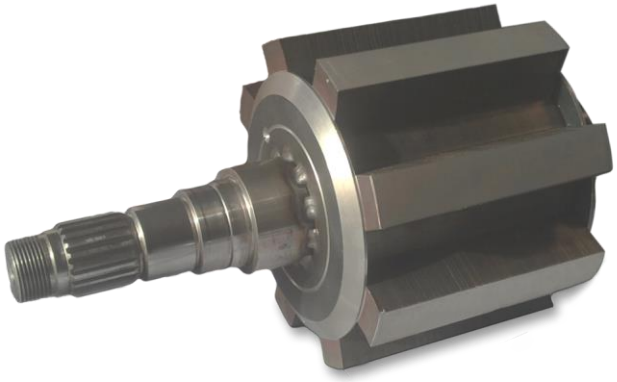

Figure 3.2.2.2 - Improved rotor design for lower disc loss

3.3 Communication

3.3.1 Private CAN

The private CAN had to be updated

- A DC link current and voltage reply message was added,
- The practical safety concept implementation introduced changes,
- A heartbeat sequence and CAN counter added to safety critical packets,
- The checksum on the application layer was removed by the use of low level CAN checksum,
- A timeout was implemented.

The consequent calculated bus load was 67.4%.

The research receives funding from the European Community Seventh Framework Programme (FP7/2007-2013) under grant agreement No 284078

3.3.2 FLEXRay

The FLEXRay communication interface with basic safety functions is functional and tested by Flanders' Drive. For the vehicle tests however, the CAN communication protocol was used.

3.4 Torque ripple

Switched reluctance motors have inherent torque ripple due to the salient stator and rotor structure. At low speed an advanced control algorithm can overcome this problem by modulating the phase currents for smooth torque output. At higher speed there is a control trade-off between motor efficiency and torque ripple and acoustic motor noise. At higher speeds, however, the effect of torque ripple is ameliorated by the higher kinetic energy of the rotating inertia.

3.4.1 Torque estimation

To understand the torque dynamics and torque ripple, a simulation model of the motor drive system behaviour with a sample time of 5 µs was developed, as shown in Figure 3.4.1.1. Indicative results are shown in Figure 3.4.1.2. No mutual coupling was included in the model.

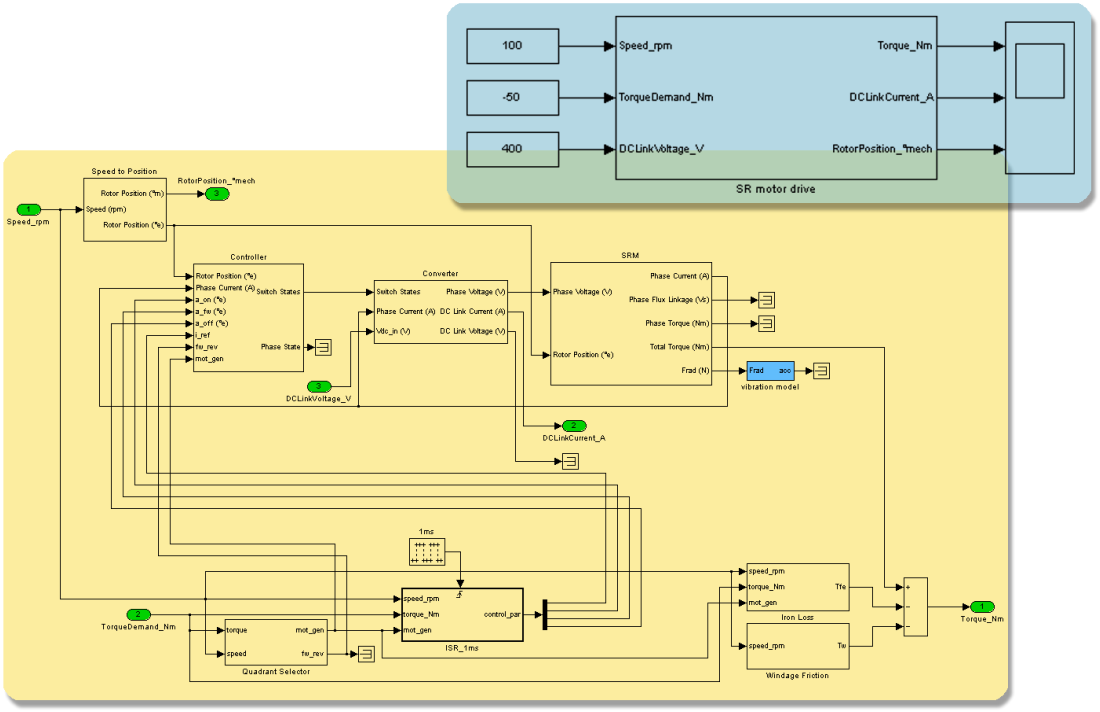

Figure 3.4.1.1 - Simulation model of motor torque, including torque ripple

The research receives funding from the European Community Seventh Framework Programme (FP7/2007-2013) under grant agreement No 284078

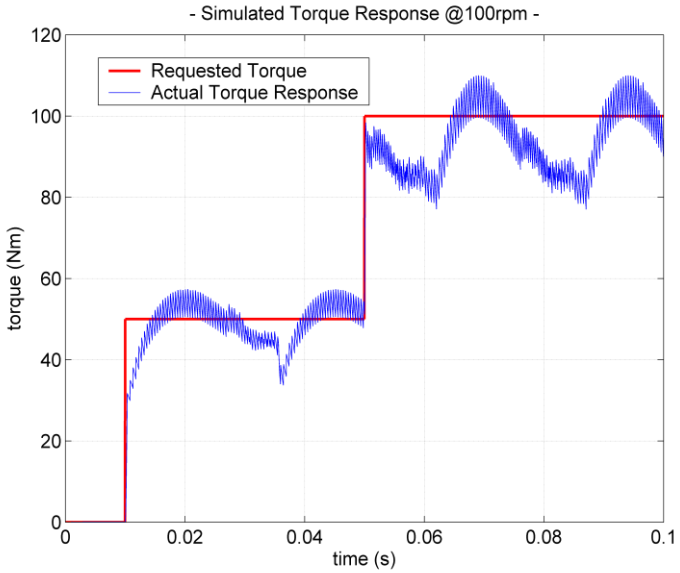

Figure 3.4.1.2 - Simulation output

3.4.2 Poor start behaviour of the vehicle demonstrator

A poor starting behaviour of the demonstrator vehicle was experienced, as shown in Figure 3.4.2.1. This was examined in the perspective of motor torque ripple.

A strong torsional vibration was identified with a frequency of 10.5Hz. This corresponds with structural resonance models of the driveline. It does not correspond with the motor torque ripple frequency, however, the structure resonance is excited by the torque ripple or changes in the torque demand.

The periodicity of the motor torque ripple is the number of phases times the number of poles, which is 24 per motor revolution. Assuming a gearbox ratio of 10.41:1 and tyres of 235/55/R19 (rolling circumference of 2.328m) the ripple frequency can be calculated (see Table 3.4.2.1.

Table 3.4.2.1 – Motor ripple frequency

Vehicle Speed	Motor Speed	Ripple frequency	
100 km/h	~7452rpm	~ 24 x 124 Hz	2981Hz
5 km/h	~ 373rpm	~ 24 x 6 Hz	149Hz

The torque ripple reduction algorithm reduced this effect, although the structural resonance characteristic is still present.

The research receives funding from the European Community Seventh Framework Programme (FP7/2007-2013) under grant agreement No.284078

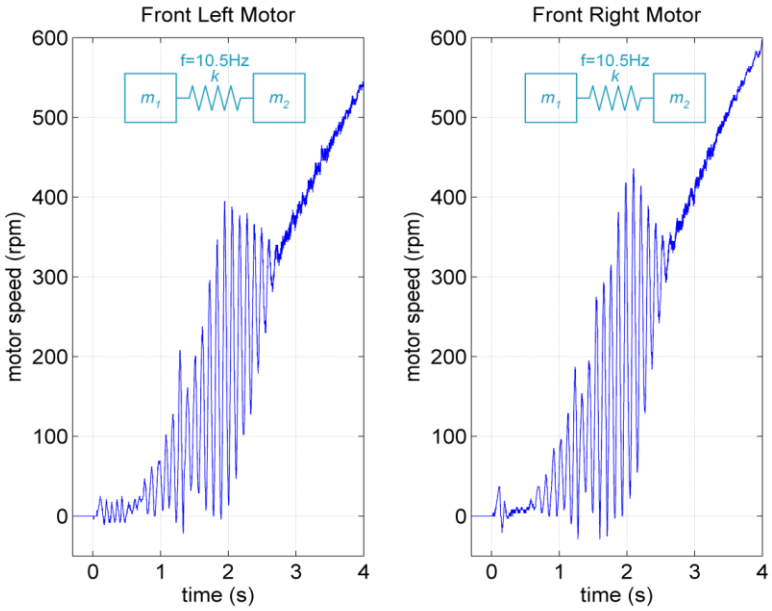

Figure 3.4.2.1 - Poor starting behaviour

Figure 3.4.2.2 shows the torque ripple improvement at low speed due to the algorithm. This was implemented and upgraded on demonstrator with an upper speed limit of the level function raised from 200 to 400 rpm. The low speed ripple was reduced from >45% to <5%.

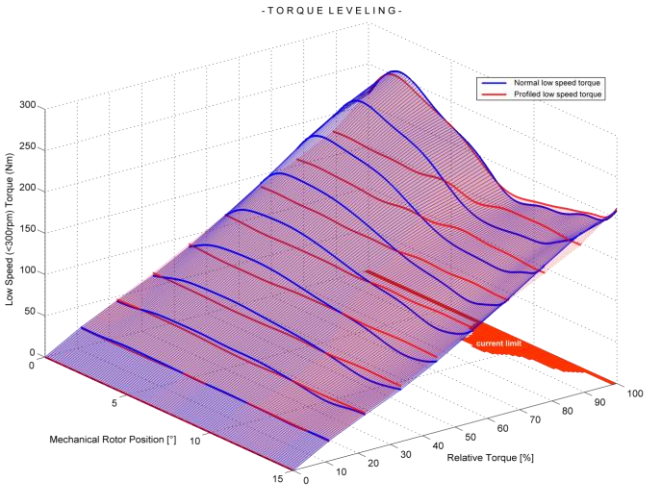

Figure 3.4.2.2 - Effect of the torque levelling function at low speed

3.5 On-line Torque estimation

Functional safety of the vehicle requires the feedback of the actuated torque, however sensing of the motor torque by a torque transducer is not feasible due to sensor cost and mechanical

The research receives funding from the European Community Seventh Framework Programme (FP7/2007-2013) under grant agreement No 284078

integration complexity. Instead, a torque estimation algorithm retransforms other sensor data to an equivalent torque on the rotor shaft.

Two methods are used:

1. Based on electrical power and motor speed.
2. Use of the phase currents instead of the dc link power.

These methods are shown in Figure 3.5.1.

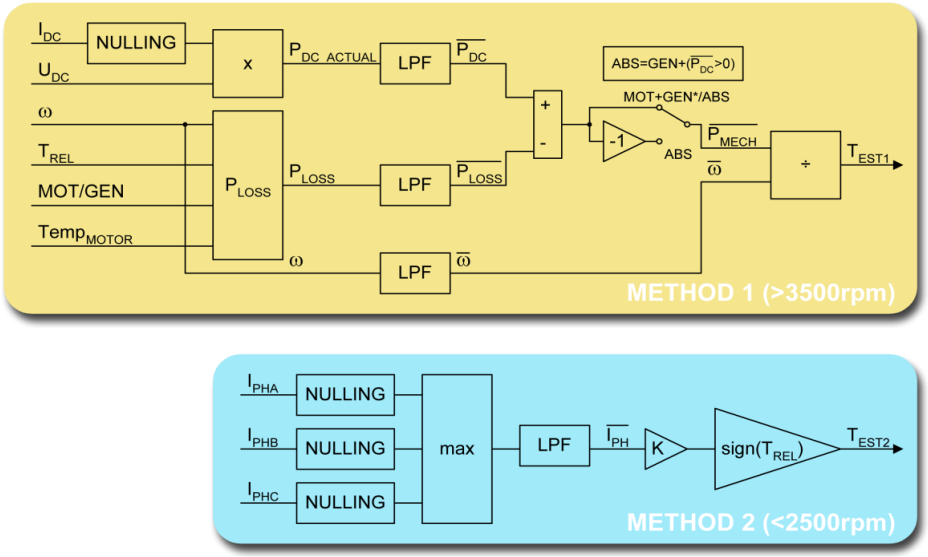

Figure 3.5.1 - Principles of torque estimation

The first method is inaccurate at low speed as shown in Figure 3.5.2.

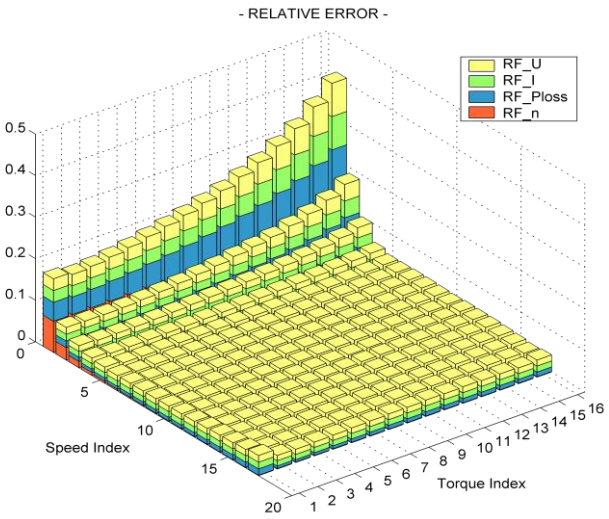

Figure 3.5.2 - Error in torque calculation method 1

The research receives funding from the European Community Seventh Framework Programme (FP7/2007-2013) under grant agreement No 284078

The second method only applies in true current control, which is restricted to rather low speed operation. Both methods are used in the vehicle and blended between 2500 and 3500 rpm of the motor shaft.

The accuracy of the final torque estimation is typically better than 15%.

3.6 Torque Mapping

The torque control function in the motor controller translates the requested MGU torque to a torque relative to the maximum at the operating speed; the torque demand, in units of Nm, is compared against the maximum torque, tabulated as function of speed, and thus expressed as a ratio. This internal torque variable is used to look up and interpolate the motor control parameters optimised for the operating voltage, for example 600 V.

Despite a reasonably accurate motor model the resultant motor torque will not exactly correspond to the MGU requested torque, due to linearity issues.

In Figure 3.6.1, the measured motoring torque map at 550 Vdc is presented up to 9000 rpm. As an example a MGU torque request of 50 Nm at 2000 rpm is investigated. First the MGU request of 50 Nm is translated into a relative torque compared to the maximum torque tabulated. At 2000 rpm this maximum torque is 192 Nm. The request of 50 Nm is thus calculated as 50 Nm / 192 Nm = 26% relative torque. The blue curves in the plot below are measured at relative torques of 11.1%, 22.2%, 33.3% ....100%. At 26% relative torque, the real torque on the shaft is about 63 Nm.

To compensate this torque non-linearity an inverse torque map is calculated for both motoring and generating condition, based on the validated maps at 550 Vdc. Two 2-dimensional lookup tables are placed in between the MGU torque request and the actual requested motor controller torque request in the Simulink program.

The research receives funding from the European Community Seventh Framework Programme (FP7/2007-2013) under grant agreement No 284078

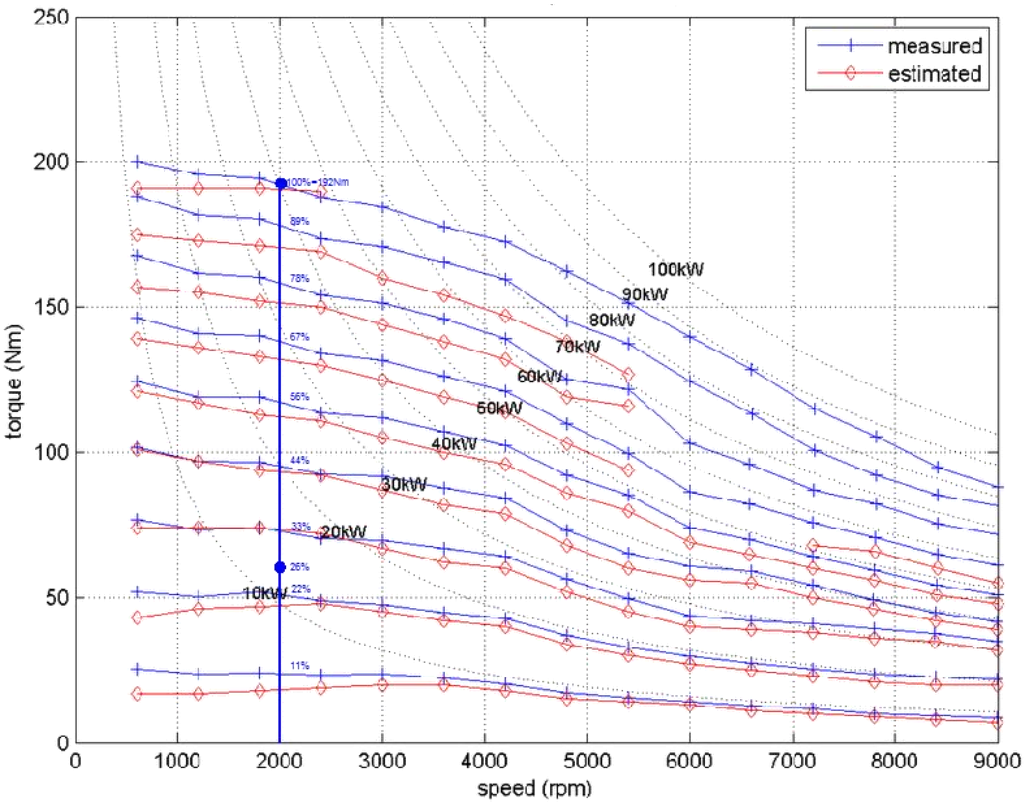

Figure 3.6.1 - Measured and estimated torque map motoring @550 Vdc

3.7 Thermal management

An on-line thermal model was developed to protect the motor when in heavy use. The principle is shown in Figure 3.7.1. The model has a sample time of 10 ms, which is evaluated during both motoring and (re)generating. It introduces an internal torque clamp function: TLIM (motor load), and is used to forecast a boost time tBOOST at peak torque TLIM. These parameters are used in the motor controller to modify the torque request signals to the motors.

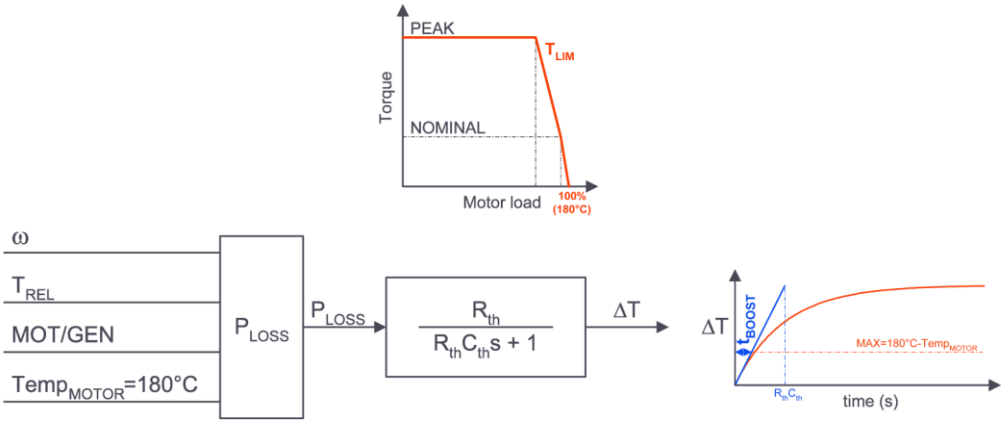

Figure 3.7.1 - Thermal management principle

The research receives funding from the European Community Seventh Framework Programme (FP7/2007-2013) under grant agreement No 284078

4 The Range Extender Trailer Concept

It was decided by consortium that the installation of a range extender into the vehicle would compromise its performance as a research platform and that more utility and learning would be gained by using available space to increase the battery voltage in the car, concentrating on the performance enhancements of the 4 wheel electric drive and accepting the limit that this would put on long periods of testing. The latter would be addressed by providing (for the testing) a mobile rapid charger unit, capable of being supplied either from a factory supply or from an internal combustion engine. By placing this combined unit in a trailer, this would allow experiments into this form of range extension to be investigated, whilst also allowing studies of the acceptability of the concept from both a customer and vehicle dynamics perspective.

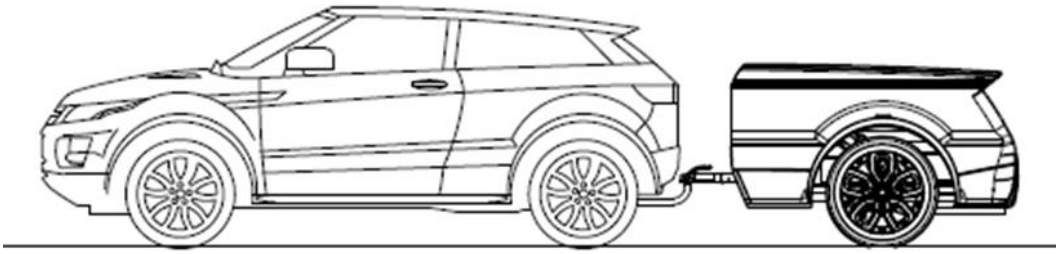

Figure 3.1 - The Range Extender Trailer Concept for the E-VECTOORC Experimental Vehicle

Targets for the range extender were set:

- 20 kW installed,
- 400-600 V delivered

The design targets were chosen to give an acceptable re-charge time for the batteries installed on the vehicle and to give a charge sustaining capability for normal driving. However, this requirement will not be used in practice on the experimental vehicle since it is only for use on test tracks.

The range extender was fabricated using bespoke frame housing a commercial generator set, together with the rapid charger adopted by the consortia.

The research receives funding from the European Community Seventh Framework Programme (FP7/2007-2013) under grant agreement No 284078

Figure 3.2 - E-VECTOORC Range Extender (Mobile Rapid Charger) in development

4.1 Electrical Equipment

The rapid charger was chosen as the CAN controlled high voltage power supply

- EDN CMP 390-02 20kW EV/HEV Charger
- Weight : 65Kg
- Size : 725 x 500 x 170mm

Figure 3.1.1- Rapid Charger

The research receives funding from the European Community Seventh Framework Programme (FP7/2007-2013) under grant agreement No 284078

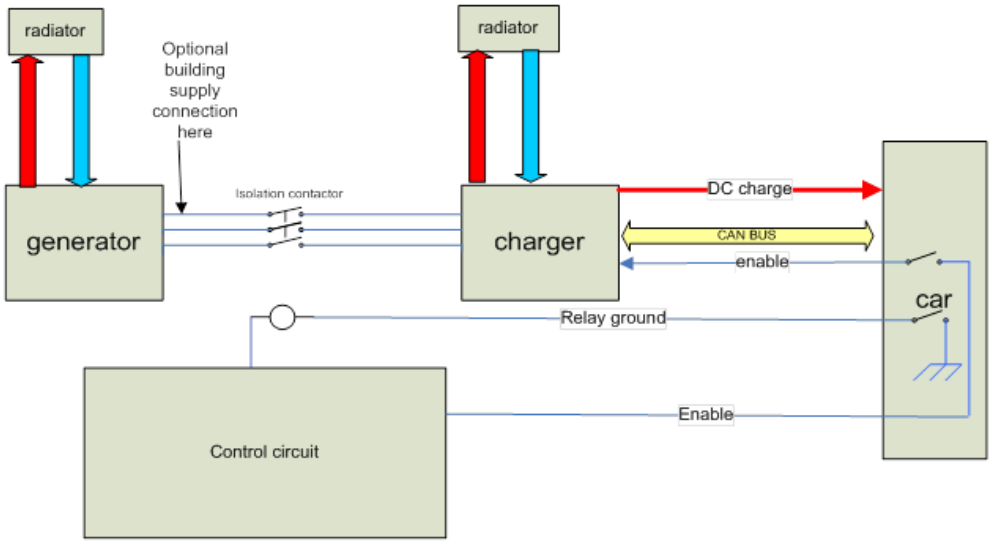

Figure 3.1.2 - Electrical Equipment

4.2 Generator Set

A variety of range extender generator sets were considered, the market moving very rapidly in this area. This varies from the extreme micro gas turbine power units (such as those proposed by Blaydon Jets [1]) through to high boost petrol engines such as those used in the CX75 concept vehicle.

It was resolved that to develop a bespoke design under the E-VECTOORC project would not be in the best interests of the consortia as the developing designs (including those at JLR) were not mature enough or cost effective enough to provide a useful test facility. Consequently, a conventional 20 kW generator set was installed in the range extender trailer.

4.3 Trailer Installation

The equipment was installed in a trailer design fabricated specifically for this task (Figure 4.3.1). Being designed for the conventional generator set, this leaves it over-engineered for development and installation of specific range extender equipment; the remaining space being aligned with the accommodation and usage requirements of a market in this field.

The research receives funding from the European Community Seventh Framework Programme (FP7/2007-2013) under grant agreement No 284078

Figure 4.3.1 - CAD Rendering of E-VECTOORC Range Extender Trailer

5 Experimental analysis of actuator dynamics in the vehicle

5.1 Introduction and objectives

The electric vehicle prototype in E-VECTOORC has two different means for torque generation at the wheels: electric torque from powertrain and friction torque from electric hydraulic brake system (SCB, Slip Control Boost from TRW modified for independent pressure control). The control system designed for the E-VECTOORC commands both sources of torque and its global performance depends on the dynamic characteristics of both types of actuators.

During WP3 and WP4, dynamic models for powertrain and electric hydraulic brake were developed. The objective in task 7.2 was the experimental analysis of their dynamic behaviour once installed on the vehicle and the validation of their simulation models.

5.2 Test plan definition and implementation

5.2.1 Electric motors

Because of the strong coupling between vehicle longitudinal dynamics and the torsional powertrain dynamics, the present analysis studies the relationship between the demand to the electric motors and the longitudinal acceleration of the vehicle. To identify the system dynamics, a sinusoidal signal is commanded simultaneously to each powertrain, sweeping

The research receives funding from the European Community Seventh Framework Programme (FP7/2007-2013) under grant agreement No 284078

frequencies between 0 and 30 Hz. Two different cases of torque level and oscillation amplitude are defined (see table 5.2.1.1).

Table 5.2.1.1 - Test cases

CASE	Type	Torque step (Nm)	Amplitude peak-to-peak (Nm)
S1	Sinusoidal	18.75	12.5
S2	Sinusoidal	37.5	25

During the controller design, an active vibration control (AVC) algorithm has been developed, in order to increase the low natural damping of the powertrain, without significantly affecting the actuator bandwidth. The present analysis includes results with both AVC enabled and AVC disabled.

Case test generation is implemented in SIMULINK/dSPACE in the E-VECTOORC controller and tests are performed on track with the FWD prototype.

5.2.2 Friction Brakes

Dynamics of the friction brakes are more independent of the vehicle longitudinal dynamics, so the analysis is focused on the relationship between pressure demand to the wheels and actual pressure in the callipers. Again, a sinusoidal signal is used for the identification, sweeping the low frequency range. Two different cases are defined (see table 5.2.2.1)

Table 5.2.2.1 - Test cases

CASE	Type	Preload (bar)	Amplitude peak-to-peak (bar)
P1	Sinusoidal	50	10
P2	Sinusoidal	100	20

Case test generation is implemented in SIMULINK/dSPACE in the E-VECTOORC controller, and tests are performed on the HIL with real brake parts.

The research receives funding from the European Community Seventh Framework Programme (FP7/2007-2013) under grant agreement No 284078

5.3 Experimental Results

5.3.1 Electric Motors

Figures 5.3.1.1 and 5.3.1.2 show the experimental results in the time and frequency domains for the electric motors both for AVC disabled and enabled. Results are presented in terms of equivalent torque, obtained from scaling the longitudinal acceleration by a factor which takes into account vehicle mass, wheel radius and powertrain ratio, so estimated torque/torque demand = 1 in static conditions. Powertrain without AVC shows very high resonance that would result in stability problems in fast modulations of the torque or when sudden torque variations occur. The damping effect of AVC is clearly shown, with a reduction of resonance peak amplitude with only slight reduction of the actuator bandwidth. The cut off frequency (defined at -3dB) for which the AVC is disabled is 15-17 Hz, whilst it is approx. 14-16 Hz for enabling the AVC.

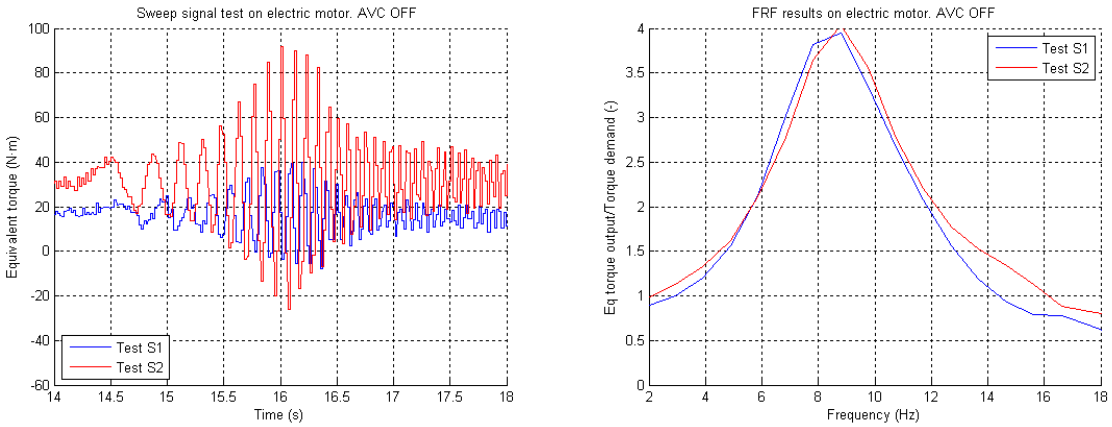

Figure 5.3.1.1 – Equivalent torque obtained from longitudinal acceleration measurements. AVC disabled

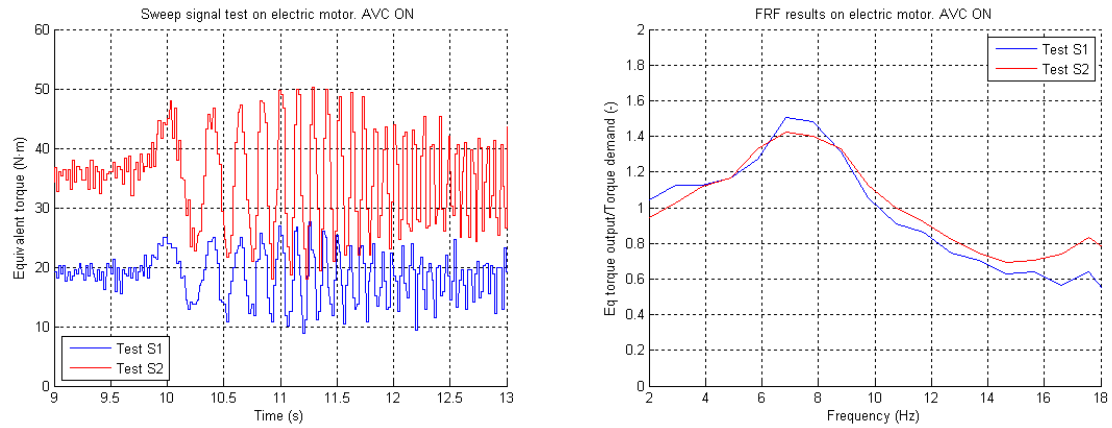

Figure 5.3.1.2 – Equivalent torque obtained from longitudinal acceleration measurements. AVC enabled

The research receives funding from the European Community Seventh Framework Programme (FP7/2007-2013) under grant agreement No 284078

The test results are compared to the powertrain model defined in previous deliverables (from WP3 and WP4). Figure 5.3.1.3 shows the comparison both for AVC ON and OFF.

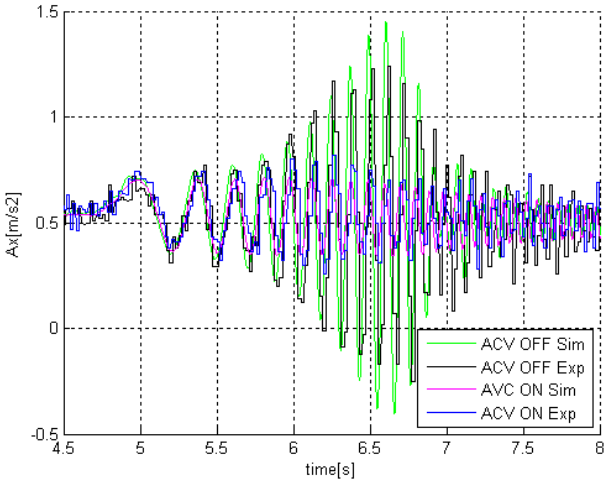

Figure 5.3.1.3 – Validation of electric powertrain model. Longitudinal acceleration for sweep signal

A good agreement is found between tests and simulations, both for cases with AVC ON and OFF.

5.3.2 Friction Brakes

Figure 5.3.2.1 shows the time domain results for the two test cases. A resonance is obtained in the range of 7 Hz with a cut off frequency in the range 12-15 Hz.

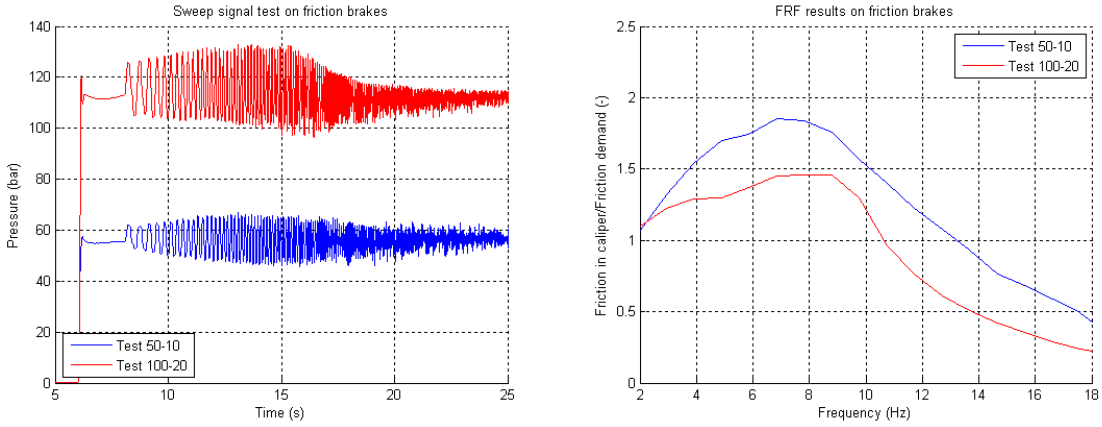

Figure 5.3.2.1 – Calliper pressure for sweep sinus input demands.

The research receives funding from the European Community Seventh Framework Programme (FP7/2007-2013) under grant agreement No 284078

Figure 5.3.2.2 plots the comparison between experimental and simulation results. In spite of the relative simplicity of the electric hydraulic brake model, significant agreement between the results is found.

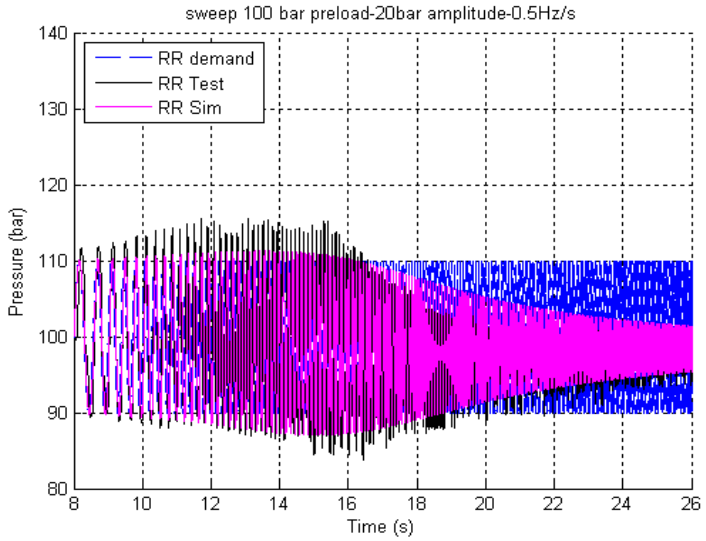

Figure 5.3.2.2 – Validation of friction brake model. Calliper pressure for sweep sinus input demand.

5.3.3 Concluding remarks

To summarise the results obtained:

- Both electric motors and friction brakes have a similar bandwidth under the tested conditions.
- Electric motors require additional damping to avoid high resonance peak. This damping can be obtained by modifying the motor demand by using AVC algorithm.
- Experimental results show that the models used in the simulation-based controller design include the relevant dynamics of both actuators.

6 Conclusion

The E-VECTOORC experimental 4 wheel drive EV has been developed and delivered, including

- Modified chasis components
- Integration of electric motors and gearboxes
- Installation of braking system

The research receives funding from the European Community Seventh Framework Programme (FP7/2007-2013) under grant agreement No.284078

- Development of range extender trailer
- Installation of measurement equipment

During commissioning tests, several issues were discovered and addressed to take the vehicle into operation. The vehicle is suitable for development of the control algorithms to establish the vehicle dynamics capability of such as a 4 individual wheel driven electric vehicle.